# Reduced BMPR2 expression induces GM-CSF translation and macrophage recruitment in humans and mice to exacerbate pulmonary hypertension

Hirofumi Sawada,[1,2,6] Toshie Saito,[1,2,6] Nils P. Nickel,[1,2,6] Tero-Pekka Alastalo,[1,2,6] Jason P. Glotzbach,[1,3] Roshelle Chan,[1,2] Leila Haghighat,[1,2] Gabriele Fuchs,[1,4] Michael Januszyk,[1,3] Aiqin Cao,[1,2,6] Ying-Ju Lai,[1,2] Vinicio de Jesus Perez,[1,5,6] Yu-Mee Kim,[1,2] Lingli Wang,[1,2,6] Pin-I Chen,[1,2,6] Edda Spiekerkoetter,[1,2,6] Yoshihide Mitani,[7] Geoffrey C. Gurtner,[1,3] Peter Sarnow,[1,4] and Marlene Rabinovitch[1,2,6]

[1]The Vera Moulton Wall Center for Pulmonary Vascular Disease, [2]Department of Pediatrics, [3]Department of Surgery, [4]Department of Microbiology and Immunology, [5]Department of Medicine, and [6]Cardiovascular Institute, Stanford University School of Medicine, Stanford, CA 94305
[7]Department of Pediatrics, Mie University Graduate School of Medicine, Mie 5148507, Japan

**Idiopathic pulmonary arterial hypertension (PAH [IPAH]) is an insidious and potentially fatal disease linked to a mutation or reduced expression of bone morphogenetic protein receptor 2 (BMPR2). Because intravascular inflammatory cells are recruited in IPAH pathogenesis, we hypothesized that reduced BMPR2 enhances production of the potent chemokine granulocyte macrophage colony-stimulating factor (GM-CSF) in response to an inflammatory perturbation. When human pulmonary artery (PA) endothelial cells deficient in BMPR2 were stimulated with tumor necrosis factor (TNF), a twofold increase in GM-CSF was observed and related to enhanced messenger RNA (mRNA) translation. The mechanism was associated with disruption of stress granule formation. Specifically, loss of BMPR2 induced prolonged phospho-p38 mitogen-activated protein kinase (MAPK) in response to TNF, and this increased GADD34–PP1 phosphatase activity, dephosphorylating eukaryotic translation initiation factor (eIF2α), and derepressing GM-CSF mRNA translation. Lungs from IPAH patients versus unused donor controls revealed heightened PA expression of GM-CSF co-distributing with increased TNF and expanded populations of hematopoietic and endothelial GM-CSF receptor α (GM-CSFRα)–positive cells. Moreover, a 3-wk infusion of GM-CSF in mice increased hypoxia-induced PAH, in association with increased perivascular macrophages and muscularized distal arteries, whereas blockade of GM-CSF repressed these features. Thus, reduced BMPR2 can subvert a stress granule response, heighten GM-CSF mRNA translation, increase inflammatory cell recruitment, and exacerbate PAH.**

CORRESPONDENCE
Marlene Rabinovitch:
marlener@stanford.edu

Abbreviations used: DRB, 5,6-dichloro-1-β-d-ribofuranosyl-benzimidazole; EC, endothelial cell; HuR, Hu-related protein R; IPAH, idiopathic PAH; LV, left ventricle; PA, pulmonary artery; PAH, pulmonary arterial hypertension; PMVEC, pulmonary microvascular EC; qRT-PCR, quantitative RT-PCR; RV, right ventricle; RVSP, RV systolic pressure; SMC, smooth muscle cell.

Idiopathic pulmonary arterial hypertension (PAH [IPAH]) is a lethal disorder characterized by obliterative changes in small- to medium-sized pulmonary arteries (PAs; Pietra et al., 1989). Familial IPAH has been linked to heterozygous germline mutations in the bone morphogenetic protein receptor 2 (BMPR2; Lane et al., 2000), but the penetrance of disease is as low as 15–20% (Newman et al., 2004). The BMPR2 mutation is therefore thought to increase susceptibility to IPAH in the context of environmental

H. Sawada's present address is Dept. of Pediatrics, Mie University Graduate School of Medicine, Mie 5148507, Japan. T.-P. Alastalo's present address is Dept. of Pediatric Cardiology, Helsinki University Hospital, Helsinki 00290, Finland. Y.-J. Lai's present address is Dept. of Respiratory Therapy, Chang Gung University College of Medicine, Taoyuan, Taiwan 333, Republic of China.



The Rockefeller University Press $30.00
J. Exp. Med. 2014 Vol. 211 No. 2 263-280
www.jem.org/cgi/doi/10.1084/jem.20111741



The Journal of Experimental Medicine

or other genetic factors (Newman et al., 2004). It is important to note that even PAH patients without a BMPR2 mutation have reduced expression of this receptor (Atkinson et al., 2002; Alastalo et al., 2011).

Inflammation is associated with IPAH; i.e., the PA lesions have elevated levels of inflammatory cytokines such as IL-1, IL-6, and TNF (Humbert et al., 1995; Itoh et al., 2006; Soon et al., 2010) and contain inflammatory cells, including macrophages, T cells, B cells, and dendritic cells (Tuder et al., 1994), and tertiary lymphoid follicles (Perros et al., 2012). Evidence for inflammation as a cause of PAH rather than a consequence has come from several sources. Recent publications show the essential role of perivascular macrophages in the pathogenesis of hypoxia-induced pulmonary hypertension (Vergadi et al., 2011), as well as interactions between activated fibroblasts and macrophages that are critical in the development of vascular pathology (Li et al., 2011). Hepatopulmonary syndrome in rats results in a proliferative pulmonary vasculopathy similar to that seen in patients that develop portopulmonary hypertension, which is completely prevented when CD68-positive macrophages are depleted (Thenappan et al., 2011). More recently, macrophages have been linked directly to endothelial apoptosis and to the development of PAH in the athymic rat in which blockade of vascular endothelial growth factor receptor (VEGFR2) is induced (Tian et al., 2013). In this model, immune reconstitution with regulatory T cells prevents the development of PAH, at least in part by enhancing the expression and activity of BMPR2 to preserve endothelial function (Tamosiuniene et al., 2011). This is consistent with experiments showing that heterozygous BMPR2 mutant mice develop PAH under inflammatory stress that does not cause PAH in control mice (Song et al., 2005). Moreover, conditional ablation of BMPR2 in PA endothelial cells (ECs [PAECs]) of transgenic mice resulted in some of the animals developing PAH, in association with perivascular infiltration of CD68-positive cells (Hong et al., 2008). Loss of function of BMPR2 in smooth muscle cells (SMCs) doubles the level of the proinflammatory cytokine IL-6 by a phospho (p)-p38–dependent signaling mechanism (Hagen et al., 2007). Moreover, mice overexpressing IL-6 develop severe PAH (Steiner et al., 2009). It was not known, however, how an increase in p38 activity could elevate levels of IL-6 or other cytokines or chemokines that recruit macrophages or other inflammatory and/or bone marrow–derived progenitor cells (Asosingh et al., 2008) that could contribute to the pathobiology of PAH (Davie et al., 2004; Frid et al., 2006).

In this study, we investigate the contribution to PAH of GM-CSF because it is a potent proinflammatory chemokine, implicated in the mobilization of ECs and other progenitor cells to sites of injury (Takahashi et al., 1999), in the expansion of myeloid-derived suppressor cells in autoimmunity (Rosborough et al., 2012) and in pulmonary hypertension (Yeager et al., 2012), in survival and activation of monocytes/macrophages (Toren and Nagler, 1998) in pulmonary hypertension (Li et al., 2011), and in the regulation of leukotriene B4 in macrophages (Serezani et al., 2012), which has been implicated in PAH (Tian et al., 2013).

## RESULTS

### GM-CSF production in PAECs and PASMCs

In human PAECs derived from central PAs, we established, by ELISA, that TNF induced a dose-dependent increase in GM-CSF production, beginning as early as 6 h after stimulation. Pretreatment with a high dose (100 ng/ml) of BMP-2 had a modest but significant inhibitory effect on TNF-induced GM-CSF production in both PAECs and PASMCs. However, when BMPR2 mRNA and protein were reduced by RNAi to <50% of the control siRNA value in PAECs (Fig. 1, A and B), TNF mediated a similar increase in GM-CSF mRNA (Fig. 1 C), but GM-CSF protein levels were enhanced by up to twofold (Fig. 1 D). This observation was confirmed with two different control (scrambled) and two different GM-CSF siRNAs (see Materials and methods). This suggested that reduced BMPR2 might be enhancing TNF-mediated GM-CSF mRNA translation. Similar findings were evident in PASMCs (not depicted). To determine whether this could be a global effect on TNF-mediated cytokine production, we also investigated changes induced in IL-6, IL-8, and MCP-1 (Fig. 1, E–J). Loss of BMPR2 also resulted in an increase in TNF-mediated p–IL-6 and IL-8 protein secretion without a comparable increase in mRNA levels. However, the TNF-mediated increase in MCP-1 mRNA and protein was unaffected by loss of BMPR2.

### Reduced BMPR2 enhanced GM-CSF mRNA translation

To assess translation of GM-CSF mRNA, we performed polysome analysis by sucrose gradient centrifugation. Effective separation of polysomes was confirmed by using Western immunoblotting to detect ribosomal subunit proteins S6 and L13a in the fractions (Fig. 2, A and B). Based on polysome profile and Western immunoblot, we divided the polysome fractions into three groups: untranslated (unbound or monosomes, fractions 1–7), moderately translated (light polysomes, fractions 8–11), and actively translated (heavy polysomes, fractions 12–15). In cells transfected with control siRNA and stimulated with TNF, 60% of the GM-CSF mRNA transcript was found in the moderately translated pool, whereas in cells with reduced BMPR2, 60% of the GM-CSF mRNA was distributed in the actively translated fraction (Fig. 2 C). Reduced BMPR2 did not affect the distribution of a housekeeping gene, GAPDH (Fig. 2 D). These data provided further evidence that impaired BMPR2 function enhances TNF-induced GM-CSF production by increasing mRNA translation. Loss of BMPR2 did not affect the stability of GM-CSF mRNA, as assessed by measuring GM-CSF mRNA levels after transcriptional inhibition by 5,6-dichloro-1-β-d-ribofuranosyl-benzimidazole (DRB; Fig. 2 E).

### Modulation of the p38–MK2 pathway by reducing BMPR2

To dissect the mechanism by which reduced BMPR2 enhances GM-CSF mRNA translation, we next assessed p38 and MK2 activity, members of a signaling pathway previously shown to be enhanced with loss of BMPR2 (Hagen et al., 2007) and to influence the transcriptional and posttranscriptional

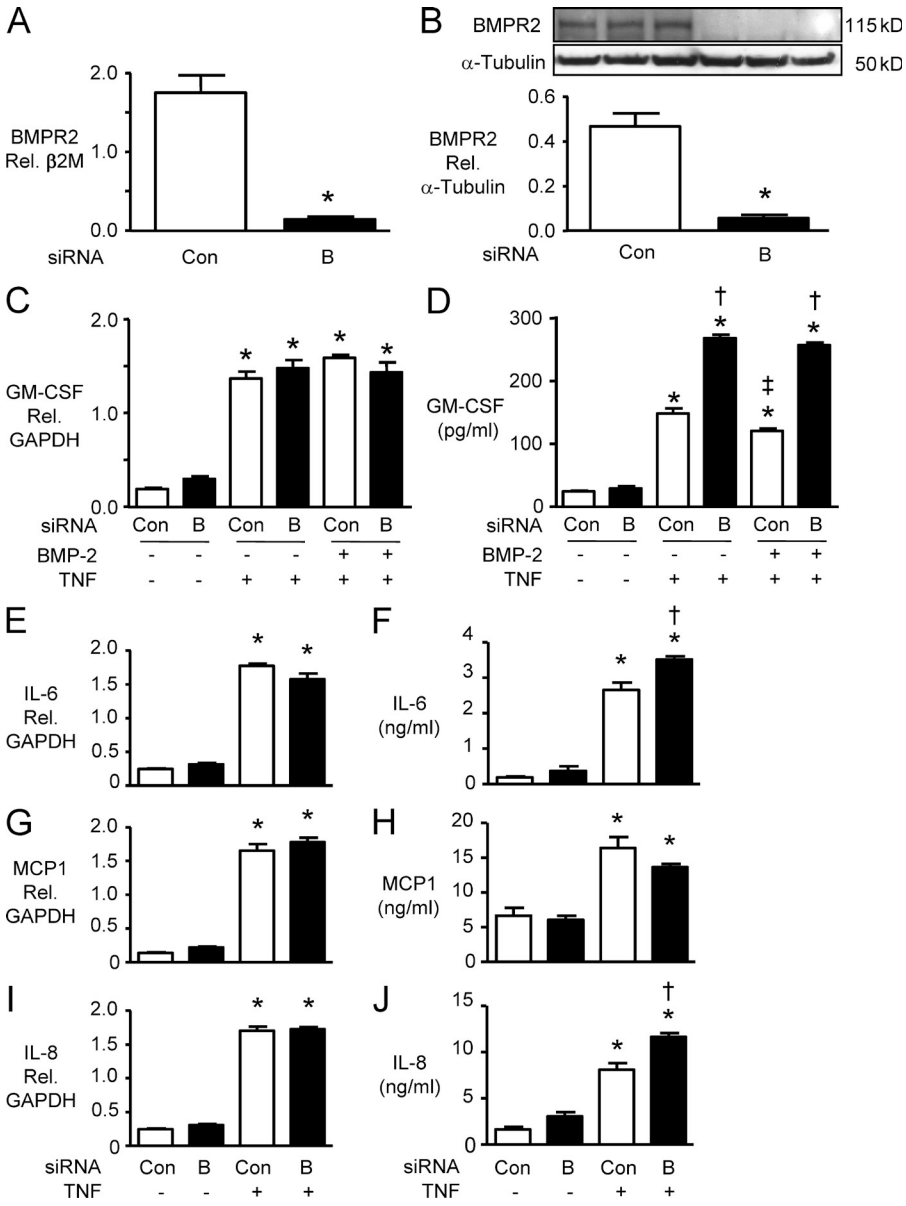


**Figure 1. GM-CSF production in PAECs.** (A and B) PAECs were transfected with BMPR2 siRNA ("B") or nontargeting siRNA as a control (Con): 48 h later, BMPR2 mRNA was measured by qRT-PCR (A) and BMPR2 protein by immunoblot (B). 24 h after transfection with B or Con siRNA, PAECs were pretreated for 30 min with 100 ng/ml BMP-2 or vehicle before adding 10 ng/ml TNF. (C and D) 6 h later, GM-CSF mRNA normalized to GAPDH was determined by qRT-PCR (C) and GM-CSF–secreted protein was measured by ELISA (D). (E–J) Similar analyses were performed for IL-6 mRNA (E) and secreted protein (F), MCP-1 mRNA (G) and secreted protein (H), and IL-8 mRNA (I) and secreted protein (J). Bars are mean ± SEM for $n = 3$ (A–D) or $n = 4$ (E–J) experiments; *, $P < 0.05$ versus Con by unpaired Student's $t$ test in A and B; *, $P < 0.05$ versus unstimulated control, matched siRNA; †, $P < 0.05$ versus Con siRNA under the same stimulation; and ǂ, $P < 0.05$ versus TNF without BMP-2 by ANOVA and Bonferroni's test of multiple comparisons in C–J.

regulation of cytokine production (Hitti et al., 2006; Anderson and Kedersha, 2008). In PAECs transfected with control siRNA, TNF induced p38 phosphorylation (p-p38) at 10 min, but the response was transient, with return to baseline levels at 30 and 60 min. However, in PAECs transfected with BMPR2 siRNA, p-p38 was sustained 30 and 60 min after TNF treatment (Fig. 3, A and B). Consistent with these results, phosphorylation of MK2 was significantly prolonged in cells transfected with BMPR2 siRNA versus control siRNA at 30 and 60 min after TNF treatment (Fig. 3, A and C). TNF-mediated activation of the transcription factor NF-κB, assessed by I-κB phosphorylation, was similar in cells transfected with BMPR2 siRNA and control siRNA (Fig. 3, A and D). When p38 and MK2 activation were inhibited using SB202190, the increase in TNF-mediated GM-CSF production in PAECs transfected with BMPR2 siRNA was reduced (Fig. 3, E and F). These results are consistent with the requirement of sustained activation of p38 mitogen-activated protein kinase (MAPK) and MK2 to enhance GM-CSF mRNA translation when there is reduced expression of BMPR2.

### Impaired stress response by reduced BMPR2

We next tested the hypothesis that the enhanced TNF-mediated GM-CSF mRNA translation in response to reduced BMPR2 is related to impaired assembly of stress granules. We first assessed the phosphorylation of eukaryotic translation initiation factor (eIF2α), a requisite modification for stress granule assembly, and observed that TNF-mediated eIF2α phosphorylation was reversed when BMPR2 levels were reduced (Fig. 4 A). The decrease in p-eIF2α associated

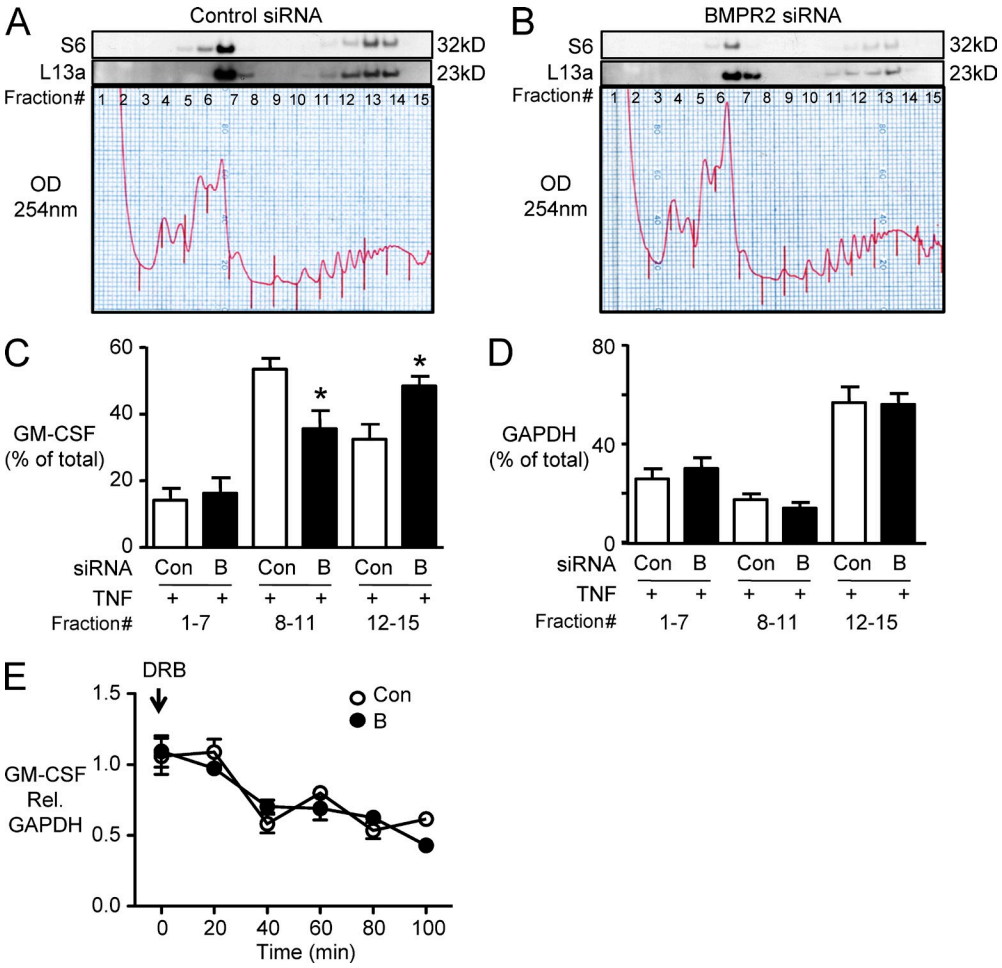


**Figure 2. Reduced BMPR2 appears to enhance GM-CSF mRNA translation.** (A and B) To assess GM-CSF mRNA translation, polysome profiles were analyzed by sucrose gradient fractionation. Similar profiles were shown for cells stimulated with TNF and transfected with Con (A) or BMPR2 siRNA (B). Western immunoblot for 40S and 60S ribosomal subunit proteins (S6 and L13a, respectively) was performed for each fraction of the sucrose gradient. GM-CSF and GAPDH mRNA were measured by qRT-PCR and expressed as the percentage of mRNA in all fractions. Fractions 1–7 lack ribosomes or contain ribosome subunits only (termed untranslated in the text). Fractions 8–11 contain light-weight polysomes (moderately translated). Fractions 12–15 contain heavy polysomes (actively translated). The experiment in A and B was repeated four times. (C and D) Bars represent mean ± SEM for $n = 3$ experiments. *, $P < 0.05$ versus TNF-stimulated and transfected with Con siRNA, all using one-way ANOVA with Bonferroni's multiple comparison test. (E) GM-CSF relative to GAPDH mRNA levels was assessed in BMPR2 siRNA (B)– and control siRNA (Con)–treated cells after TNF stimulation as described in the Materials and methods at the indicated time points after DRB to assess changes in mRNA stability. Symbols represent mean ± SEM of $n = 4$ assessed by ANOVA.

with reduced levels of BMPR2 was p-p38 dependent, as it was lost when p-p38 was inhibited by SB202190 (Fig. 4 B). We then investigated whether p38 activation enhanced phosphatase activity, necessary to dephosphorylate eIF2α and promote mRNA translation. The GADD34–PP1 complex dephosphorylates eIF2α, but we found no change in the levels of GADD34 or PP1 (Fig. 4 C) or in the amount of complex formed (Fig. 4 D) in response to reduced BMPR2 and prolonged p-p38. However, salubrinal, a chemical inhibitor of GADD34–PP1 activity, reversed both the dephosphorylation of eIF2α (Fig. 4 E) and the enhanced GM-CSF production (Fig. 4 F) associated with reduced BMPR2. Decreasing PP1 by siRNA (Fig. 4 G) also reversed the enhanced GM-CSF production observed in TNF-stimulated PAECs with reduced levels of BMPR2 (Fig. 4 H). Collectively, our experiments support a model in which loss of BMPR2 prolongs p-p38 activity required for GADD34–PP1 activity, and this dephosphorylates eIF2α and impairs assembly of stress granules facilitating GM-CSF mRNA translation.

To further assess stress granule assembly in PAECs with and without loss of function of BMPR2 by immunofluorescence microscopy, we first costained the RNA binding proteins TIA-1 and Hu-related protein R (HuR), associated with stress granules under conditions of TNF stimulation. Arsenite was used as a positive control for stress granules (Fig. 5, A–H). Additional experiments were performed using G3BP as a marker for stress granules. 3 h after the addition of TNF or

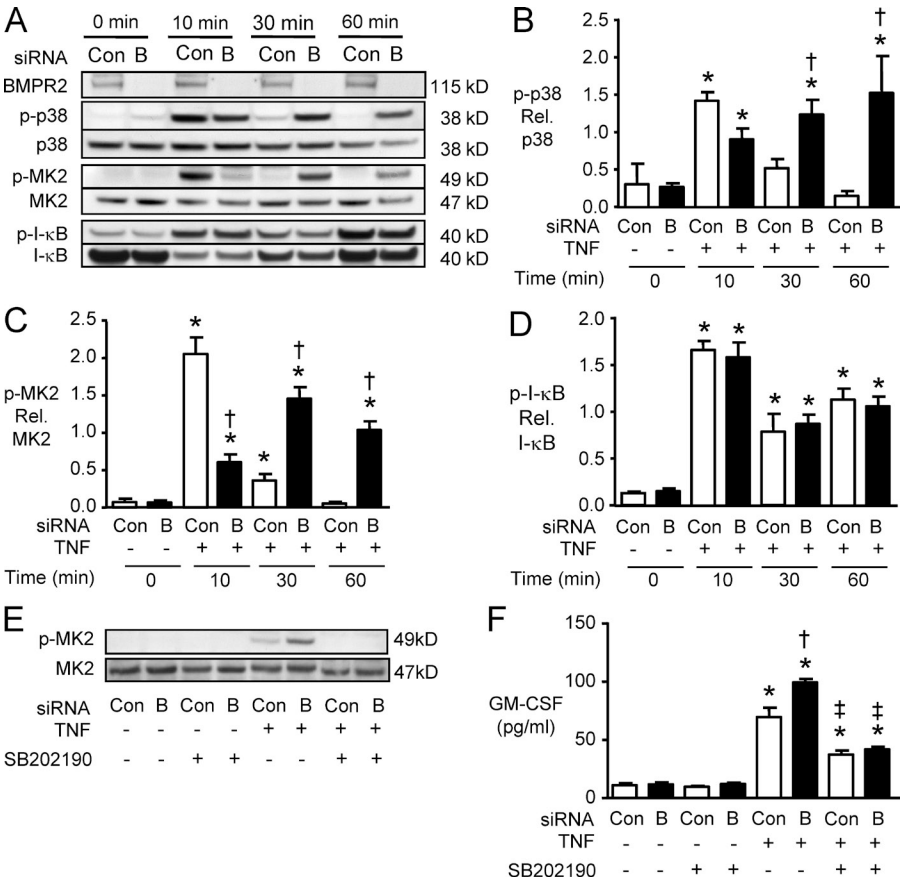


**Figure 3. Reduced BMPR2 induces sustained activation of p38 and MK-2.** (A) Representative Western immunoblots for BMPR2, p-p38, total p38, p-MK2, total MK2, p–I-κB, and total I-κB in PAECs transfected with BMPR2 siRNA ("B") or control siRNA (Con), 10, 30, and 60 min after stimulation with 10 ng/ml TNF. (B–D) Densitometric analysis of the immunoreactive bands for p38 (B), MK-2 (C), and I-κB (D). Bars are means ± SEM for $n = 3$ experiments. *, $P < 0.05$ versus unstimulated control; †, $P < 0.05$ versus cells transfected with Con siRNA, using ANOVA with Bonferroni's multiple comparison test. (E and F) 24 h after transfection, PAECs were pretreated for 30 min with 3 µM SB202190 or DMSO and then stimulated with 10 ng/ml TNF or vehicle (saline). (E) Representative immunoblot for p-MK2 levels 30 min after TNF. (F) GM-CSF by ELISA, 6 h after treatment with TNF or vehicle. Bars are mean ± SEM for $n = 4$ experiments. *, $P < 0.05$ versus unstimulated control; †, $P < 0.05$ versus stimulated Con siRNA (Con); ǂ, $P < 0.05$ SB202190 versus DMSO pretreated, all by ANOVA with Bonferroni's multiple comparison test.

exposure to hypoxia (1% $O_2$; Brown et al., 2011), abundant stress granules appeared (Fig. 5, I–P). In all conditions studied (TNF, arsenite, and hypoxia), loss of BMPR2 significantly reduced stress granule formation.

### GM-CSF protein is increased in IPAH versus donor control lungs

To establish the clinical significance of our findings in patients with IPAH, Western immunoblot for GM-CSF was performed on whole lung tissue from 10 IPAH patients and 8 control unused donor lungs (Tables 1 and 2 provide clinical and demographic information on the population studied). Elevated levels of GM-CSF were observed in the IPAH versus control samples (Fig. 6, A and B). We then localized the heightened expression of GM-CSF protein using immunohistochemistry. GM-CSF protein was not readily detected in the PAs of unused donor control lungs (Fig. 6 C), but there was moderate to intense GM-CSF immunoreactivity in the endothelium, thickened intima, and hypertrophied media of the PAs of the IPAH patients (Fig. 6, D–F). GM-CSF co-distributed with increased immunoreactivity for TNF in IPAH PAs (Fig. 6, D–F). There was also minimal if any detection of TNF protein in control PAs (Fig. 6 C). Semiquantitative analysis for GM-CSF immunoreactivity (not depicted) indicated statistically significant differences in GM-CSF and TNF expression in IPAH versus control vessels of the same size and location.

### GM-CSF receptor α (GM-CSFRα) immunoreactivity in the lungs of IPAH patients

As GM-CSF can recruit inflammatory and progenitor cells to the vessel wall, we assessed the distribution and nature of GM-CSFRα–expressing cells in the PAs of IPAH patients by immunohistochemistry and by microfluidic-based single cell transcriptional analysis. In the donor control lungs, GM-CSFRα immunoreactivity was not detectable in the PAs but was seen in alveolar macrophages (Fig. 7 A). In the IPAH patient lung tissues, GM-CSFRα co-distributed with cells expressing CD31 and CD68 in the thickened intima, in the media, and in neoangiogenic channels in plexiform lesions (Fig. 7, B and C).

Consistent with the immunohistochemical analyses, flow cytometry of freshly isolated lung CD31-positive cells revealed that the fraction of GM-CSFRα–positive cells was significantly expanded in IPAH versus unused donor control lungs (77.4 ± 17 vs. 20.9 ± 12%, $P < 0.05$; Fig. 7, D and E). Single cell transcriptional analysis using microfluidic-based real-time quantitative RT-PCR (qRT-PCR) identified two subpopulations with distinct transcriptional signatures. 46% of the cells were assigned membership to a

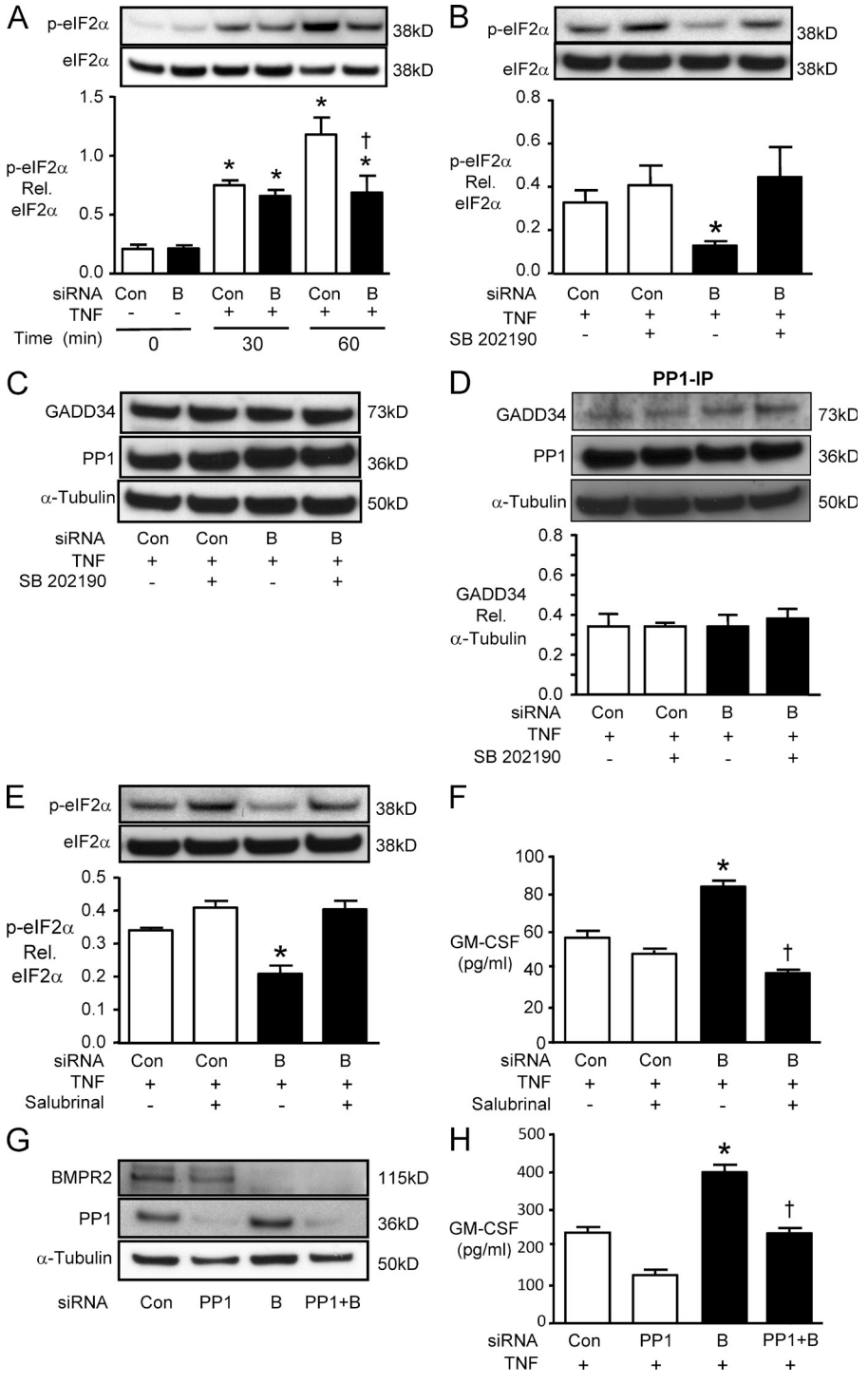


**Figure 4. Reduced BMPR2 inhibits eIF2α phosphorylation in a p-p38– and PP1-dependent manner.** (A) PAECs were transfected with BMPR2 ("B") or control siRNA (Con) and harvested either before (0) or 30 and 60 min after TNF stimulation. Phosphorylation of the α subunit of eIF2α analyzed by Western immunoblot is shown above with densitometry below. Bars are mean ± SEM for $n = 3$ experiments. *, $P < 0.05$ versus unstimulated control; †, $P < 0.05$ versus cells transfected with Con siRNA under the same condition by ANOVA with Bonferroni's multiple comparison test. (B) 24 h after transfection with B or Con siRNA, PAECs were pretreated with 3 μM SB202190 or DMSO (vehicle) for 30 min before stimulation with 10 ng/ml TNF. 60 min later, phosphorylation of eIF2α was analyzed by Western immunoblot and densitometric analysis. (C) Representative immunoblots of GADD34 and PP1 60 min after TNF treatment in the presence or absence of the p-p38 inhibitor SB202190. (D) PP1 was immunoprecipitated, and GADD34 was measured by Western immunoblot and normalized for tubulin in the initial sample. (E) 24 h after B or Con siRNA, PAECs were pretreated with 75 μM Salubrinal or DMSO (vehicle) for 30 min before adding 10 ng/ml TNF; 60 min later, p-eIF2α was assessed. (F) Secreted GM-CSF by ELISA 6 h after TNF in the presence or absence of Salubrinal. For B, D, and E, bars are mean ± SEM for $n = 3$ experiments; for F, $n = 4$ experiments. *, $P < 0.05$ versus Con siRNA untreated; †, $P < 0.05$ versus DMSO (vehicle)-treated cells transfected with BMPR2 siRNA by ANOVA with Bonferroni's multiple comparison test. (G) Representative Western immunoblot for BMPR2 and PPI after control, PPI, BMPR2 (B), and PPI + BMPR2 (PPI + B) siRNA. (H) Secreted GM-CSF levels by ELISA 6 h after TNF stimulation. Bars are mean ± SEM for $n = 4$. *, $P < 0.05$ versus Con siRNA; †, $P < 0.05$ versus BMPR2 siRNA.

subpopulation with high expression of other endothelial genes, including VWF, KDR, TEK, ENG, and CD34 (Fig. 7 F, left), and the remaining 54% of the cells comprised a different subpopulation with high expression of monocyte/macrophage-associated genes, including CD14, CD68, CD163, vimentin, and CD44 (Fig. 7 F, right). The proportion of GM-CSFRα–positive cells expressing monocyte/macrophage markers was considerably higher in the IPAH lungs than in the control tissue, i.e., 35 versus 3.5% (not depicted). These experiments suggest a strong association between elevated levels of GM-CSF and the recruitment of GM-CSFRα–positive cells that could be of endothelial or hematopoietic lineage. There was no evidence that GM-CSF at doses of 0.1–10 ng/ml could appreciably induce proliferation of cultured

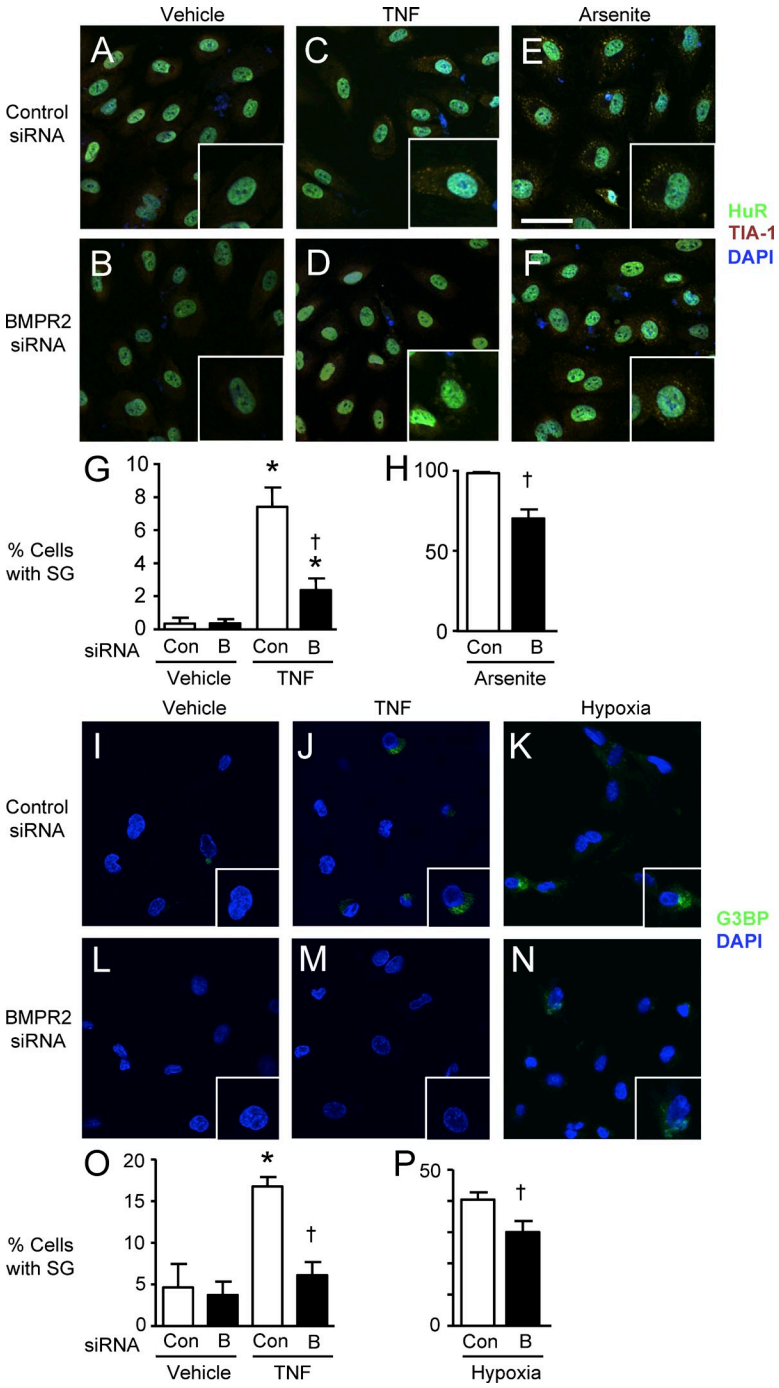


**Figure 5. Stress granule formation was inhibited by reduced BMPR2.** (A–F) 24 h after transfection with control siRNA (Con; A, C, and E) or siRNA for BMPR2 ("B"; B, D, and F) PAECs were stimulated with 10 ng/ml TNF or vehicle for 3 h or with 0.5 mM arsenite for 45 min. Cells were fixed in 4% paraformaldehyde and incubated with mouse monoclonal anti-HuR and goat polyclonal anti–TIA-1 antibodies (1:200) labeled with Alexa Fluor 488 (for HuR)–conjugated anti–mouse and Alexa Fluor 594 (for TIA-1)–conjugated anti–goat secondary antibodies. DAPI was used to label cell nuclei. (A–F) Representative confocal images of vehicle-treated cells (A and B), TNF-treated cells (C and D), and arsenite-treated cells (E and F) with high-magnification insets showing double immunofluorescent stress granules in the cytoplasm. Bar, 20 µm. (G and H) Quantification of stress granule (SG) formation. Cells with stress granules were counted in three randomly chosen microscopic fields (×200). Bars are the mean ± SEM of four different experiments. *, $P < 0.05$ versus unstimulated control; †, $P < 0.05$ versus cells transfected with control siRNA under the same condition by ANOVA with Bonferroni's multiple comparison test (G) or unpaired Student's *t* test (H). (I–N) A similar experiment with G3BP as the readout for stress granule formation with vehicle (I and L), TNF (J and M), and 1% hypoxia for 3 h (K and N). High-magnification insets are shown. Same scale as in A–F. (O and P) Percentage of cells with stress granules was calculated as described for G and H. Bars are the mean ± SEM for $n = 4$. *, $P < 0.05$ versus control siRNA; and †, $P < 0.05$ versus control siRNA under the same condition, by ANOVA and Bonferroni's multiple comparison test (O) or unpaired Student's *t* test (P).

PAECs or PASMCs (not depicted), so we propose that its major function may lie in recruiting cells that could contribute to vascular pathology.

### GM-CSF exacerbates and GM-CSF blockade prevents chronic hypoxic PAH in mice

To determine whether up-regulation of the GM-CSF–GM-CSFRα axis induces or increases the severity of PAH, we administered murine GM-CSF to mice exposed to room air or to chronic hypoxia for 3 wk, as described in the Materials and methods. GM-CSF administration negatively impacted body weight in mice exposed to chronic hypoxia for 3 wk (Table 3). The total number of circulating white blood cells tended to be higher in the GM-CSF–treated group but did not reach statistical significance; the proportion of neutrophils and monocytes was, however, greater in the GM-CSF–treated mice (Tables 1 and 2). Hematocrit was, as expected, higher in hypoxic animals but was unaffected by GM-CSF administration. Left ventricle (LV) function and cardiac output were unaffected by GM-CSF treatment (Tables 1 and 2).

**Table 1.** Patient characteristics for unused donor controls in the immunohistochemical study

| Pt | Age | Gender | Cause of death |
|---|---|---|---|
| | *yr* | | |
| 1 | 25 | Male | Gunshot wound to the head |
| 2 | 12 | Male | Brain death, diabetic ketoacidosis |
| 3 | 60 | Male | Brain death, aortic dissection |
| 4 | 54 | Male | Choking with anoxic brain injury |
| 5 | 41 | Female | Subarachnoid hemorrhage |
| 6 | 17 | Male | Head injury |
| 7 | 49 | Male | Intracranial hemorrhage |
| 8 | 18 | Male | Gunshot wound to the head |

However, right ventricle (RV) systolic pressure (RVSP) was significantly higher in the GM-CSF– versus vehicle-treated group after exposure to hypoxia (Fig. 8 A), consistent with more severe RV hypertrophy (Fig. 8 B). Morphometric analysis using barium-injected lung tissues revealed that the percentage of muscularized small PAs induced by chronic hypoxia was also significantly higher in GM-CSF–treated animals (Fig. 8, C and D), but the reduced number of distal arteries per 100 alveoli was unchanged by GM-CSF administration (Fig. 8 E). Immunohistochemistry revealed a significantly higher number of perivascular cells expressing a macrophage marker (Mac-3) in GM-CSF–treated room air animals, similar to that seen with hypoxic exposure. The combination of GM-CSF and hypoxia was additive in recruiting perivascular Mac-3–positive cells (Fig. 8, F and G).

Given that recruitment of macrophages in hypoxia was evident both in our experiments and in those recently reported (Vergadi et al., 2011), we determined whether blocking GM-CSF might prevent hypoxia-induced pulmonary hypertension. Injection of a GM-CSF–neutralizing antibody prevented hypoxia-induced pulmonary hypertension, RV hypertrophy, and associated vascular changes described above, including recruitment of perivascular macrophages (Fig. 8).

To determine whether GM-CSF might also be elevated in an inflammatory model of PAH, we monitored its expression using qRT-PCR in rats injected with the toxin monocrotaline as described in the Materials and methods. We observed an almost twofold increase in mRNA levels for GM-CSF in the lungs of rats at 14 d after injection of monocrotaline (Fig. 8 H), a time point we and others have shown is consistent with the development of significant pulmonary hypertension in this model (Rosenberg and Rabinovitch, 1988).

## DISCUSSION

Clinical and experimental studies have linked reduced expression of BMPR2 with inflammation and PAH (Song et al., 2005; Hagen et al., 2007; Hong et al., 2008). Our study has uncovered a novel mechanism accounting for this link. We have shown that in response to a proinflammatory cytokine such as TNF, prolonged activation of p38–MK2 occurs if there is reduced expression of BMPR2. This activates GADD34–PP1 and dephosphorylates eIF2α, thereby impairing assembly of stress granules and enhancing mRNA translation of GM-CSF along with a subset of TNF-mediated cytokines that likely includes IL-6 and IL-8 but not MCP-1. In addition to mRNA translation, the level of secreted cytokine depends on factors that stabilize or destabilize the protein.

We show, for the first time to our knowledge, the involvement of GM-CSF in the pathobiology of pulmonary vascular lesions in IPAH patients. Heightened GM-CSF co-distributes with increased immunoreactivity for TNF throughout the vessel wall in patients with IPAH and is associated with an expanded subpopulation of intimal cells positive for GM-CSFRα. We determined by microfluidic-based single cell transcriptional analysis that these cells were divided equally into two subgroups; one subgroup coexpressed markers of ECs, and the other subgroup coexpressed markers of monocytes/macrophages. Moreover, we provide evidence that administration of GM-CSF can worsen pulmonary hypertension in mice exposed to hypoxia, in association with enhanced recruitment of perivascular macrophages, and that blockade of GM-CSF

**Table 2.** Patient characteristics for IPAH in the immunohistochemical study

| Pt | Age | Gender | PAP (s/d/m) | PVR | 6MW | Medication |
|---|---|---|---|---|---|---|
| | *yr* | | *mmHg* | $dyn \times s \times cm^{-5} \times m^2$ | | |
| 1 | 58 | Female | 66/37/50 | 685 | 298 | Bosentan, Epoprostenol, Sildenafil, Treprostinil |
| 2 | 7 | Male | 143/82/105 | 2,226 | 256 | Bosentan, Epoprostenol, Sildenafil |
| 3 | 43 | Male | 55/35/40 | 756 | 272 | Bosentan, Sildenafil, Iloprost |
| 4 | 47 | Female | 82/36/51 | 1,103 | 121 | Bosentan, Epoprostenol, Sildenafil, Treprostinil |
| 5 | 10 | Female | 103/43/62 | 1,400 | 460 | Bosentan, Sildenafil, Iloprost, Treprostinil, Imatinib |
| 6 | 15 | Female | 175/66/102 | 2,018 | 387 | Epoprostenol, Sildenafil |
| 7 | 16 | Female | 125/72/95 | 3,238 | 512 | Bosentan, Epoprostenol, Sildenafil, Treprostinil |
| 8 | 24 | Male | 113/70/88 | 1,356 | 182 | Bosentan, Epoprostenol, Sildenafil |
| 9 | 62 | Female | 67/22/37 | 1,018 | 278 | Bosentan, Epoprostenol, Sildenafil |
| 10 | 38 | Female | 89/26/50 | 1,170 | 288 | Bosentan, Sildenafil |

PAP, PA pressure (s, systolic; d, diastolic; m, mean); PVR, pulmonary vascular resistance; 6MW, distance (m) walked in 6 min.

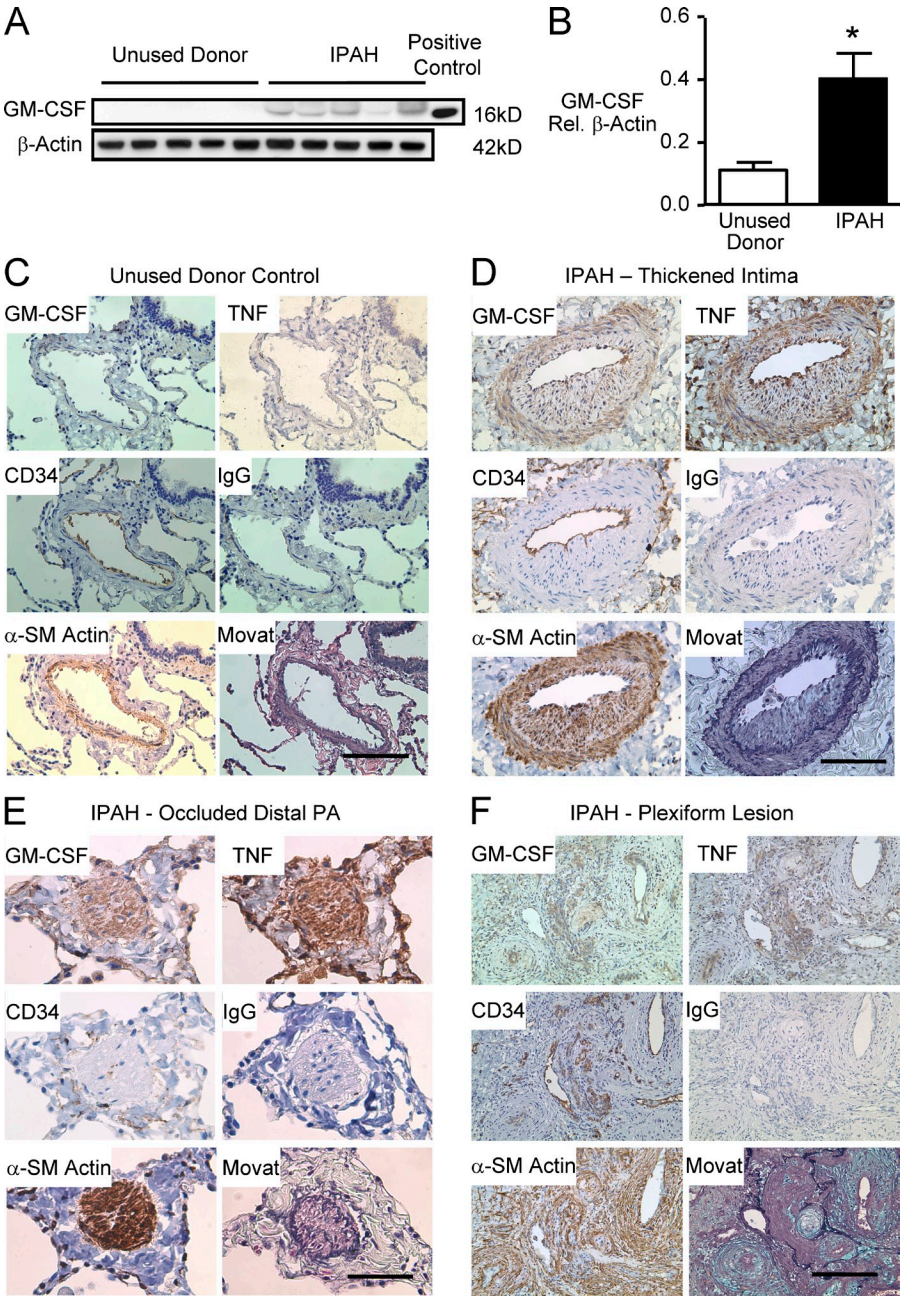


**Figure 6. Increased GM-CSF protein in lungs of IPAH patients versus unused donor control lungs.** (A) Representative immunoblots for GM-CSF using lung tissue from five IPAH patients and five unused donor control lungs. (B) Densitometric analysis of Western immunoblots for GM-CSF from lung tissue of 10 IPAH patients and 8 controls. Bars are mean ± SEM. *, $P < 0.05$ versus unused donor control lungs by unpaired Student's *t* test. (C–F) Representative immunohistochemistry for GM-CSF, CD34, α-SM–actin, and TNF in a PA from a control (C) and IPAH lung (D–F): PA intima thickness (D), a distal small PA (E), and plexiform (F). Bars: (C and D) 100 µm; (E) 50 µm; (F) 250 µm. Co-distribution of intense immunoreactivity for GM-CSF and TNF is seen in the endothelium, intima, and media of the IPAH vessel wall.

prevents this pathology. In addition, elevated GM-CSF coincides with the development of significant pulmonary hypertension in rats in response to the proinflammatory agent monocrotaline. Collectively, our experiments provide a novel mechanistic link between PAH, reduced expression of BMPR2, and an amplified response to a proinflammatory signal that promotes GM-CSF–mediated recruitment of cells that can contribute to pulmonary vascular pathology by their production of cytokines, chemokines, leukotrienes, proteolytic enzymes, and growth factors.

Several previous studies support the antiinflammatory properties of BMPR2 signaling (Song et al., 2005; Hagen et al., 2007; Hong et al., 2008). To further address the proinflammatory effects of loss of BMPR2 signaling, we stimulated cells with TNF because high circulating levels of this cytokine are evident in patients with IPAH (Itoh et al., 2006; Soon et al., 2010). Moreover, TNF can induce PAH in experimental animals, albeit in association with severe emphysema (Fujita et al., 2002) or related to heightened vasoreactivity (Stevens et al., 1992). The response to TNF is the induction of a cytokine/chemokine cascade involving GM-CSF (Crane et al., 1999). Loss of BMPR2, however, greatly amplified TNF-mediated GM-CSF production by a mechanism that we related to p-p38–dependent impaired stress granule assembly and mRNA translation.

It has been reported that MK2, a substrate of p-p38, plays a critical role in the posttranscriptional as well as the transcriptional

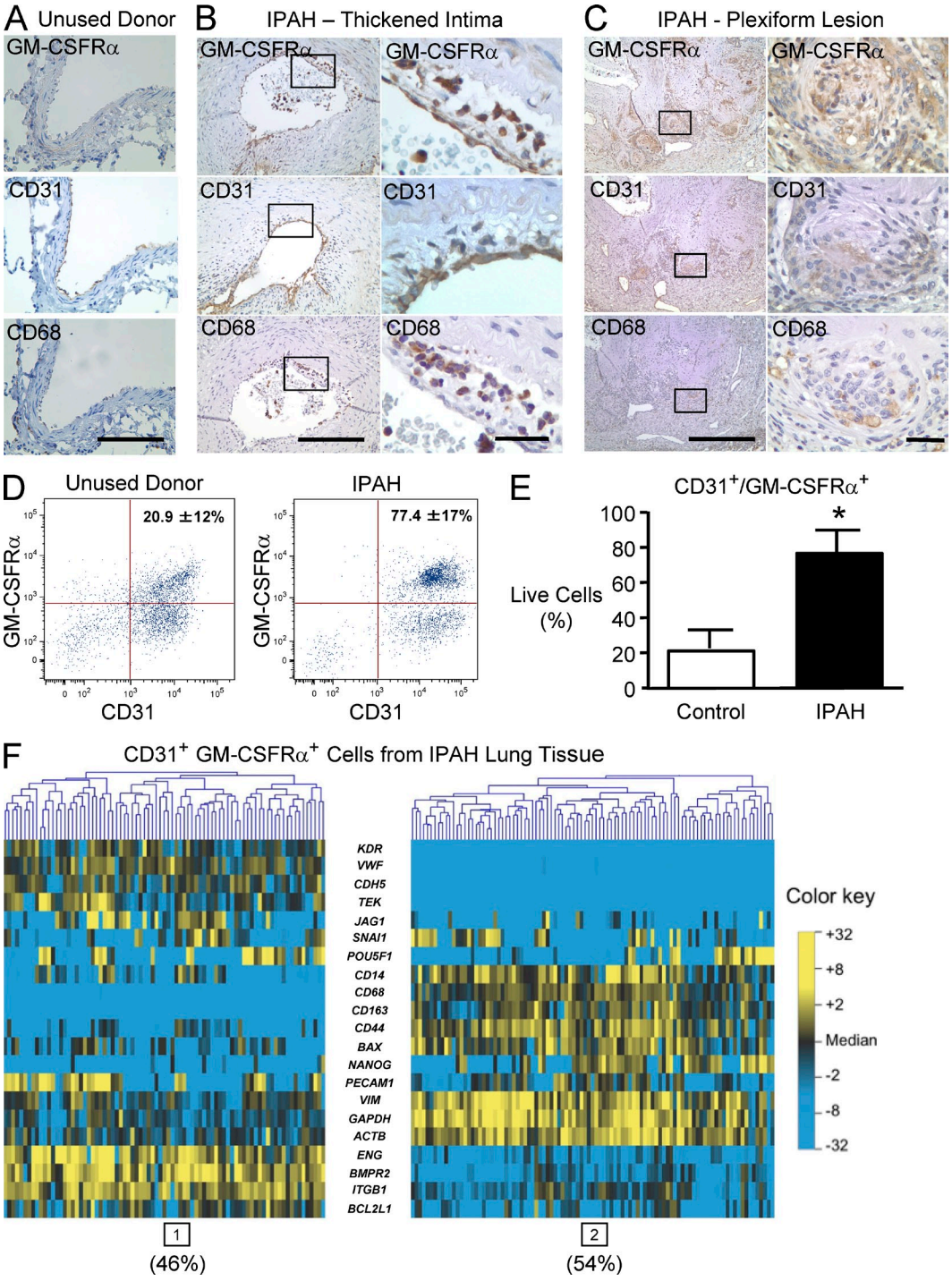


**Figure 7. GM-CSFR–positive cells are expanded in IPAH lungs.** (A–C) Immunohistochemistry for GM-CSFRα, CD31, and CD68. (A) PA from control. (B) PA intima thickness. (C) Plexiform. Boxed areas are shown at higher magnification in the panels on the right. Bars (A) 100 µm; (B, left) 200 µm; (C, left) 500 µm; (B and C, right) 25 µm. Co-distribution of GM-CSFRα immunoreactivity and CD31-positive cells lining the vessel lumen and that are CD68 positive in the neointima. (D) Representative FACS analysis of freshly isolated cells from the lung tissues of an unused donor (left) and an IPAH patient (right) and sorted for immunofluorescence using CD31 and GM-CSFRα antibodies as described in the Materials and methods. (E) Percentage of $CD31^+GM\text{-}CSFR\alpha^+$ cells in IPAH versus unused donor control lungs. Bars indicate mean ± SEM. $n = 3$; *, $P < 0.05$ determined by unpaired Student's $t$ test. (F) Microfluidic-based single cell transcriptional analysis of $CD31^+GM\text{-}CSFR\alpha^+$ cells pooled from three IPAH patients. Gene expression is represented on a color scale from yellow (high) to blue (low). Gene expression data for individual cells are oriented in vertical columns. Two subpopulations are evident: endothelial (high expression of endothelial/vascular genes; cluster 1, 46% of cells) and hematopoietic (high expression of monocyte/macrophage markers; cluster 2, 54% of cells).

**Table 3.** Body weight and hematological and echocardiographic findings in mice

| Parameter | Room air | | Hypoxia | |
|---|---|---|---|---|
| | Saline | GM-CSF | Saline | GM-CSF |
| **Final body weight (g)** | 24.41 ± 0.97 (9) | 23.56 ± 0.78 (9) | 22.38 ± 0.69 (14) | 20.39 ± 0.65 (14)[a] |
| **Hematological study** | | | | |
| White blood cell (/μl) | 4,699 ± 480 (7) | 6,806 ± 1,115 (7) | 3,455 ± 390 (8) | 5,098 ± 943 (8) |
| Neutrophil (%) | 14.2 ± 4.82 (6) | 25.3 ± 5.5 (6) | 5.6 ± 0.84 (7) | 21.96 ± 4.66 (7)[b] |
| Lymphocyte (%) | 80.8 ± 4.62 (6) | 65.0 ± 7.45 (6) | 92.6 ± 1.24 (7) | 73.7 ± 6.17 (7)[b] |
| Monocyte (%) | 2.2 ± 0.54 (6) | 5.7 ± 1.28 (6)[b] | 1.4 ± 0.20 (7) | 2.9 ± 0.54 (7)[b] |
| Hematocrit (%) | 43.9 ± 0.67 (7) | 46.5 ± 0.96 (7) | 59.2 ± 0.72 (8)[a] | 59.4 ± 1.58 (8)[a] |
| Serum GM-CSF (pg/ml) | ND | 17.3 ± 5.2 (4) | ND | 13.27 ± 4.90 (4) |
| **Echocardiographic study** | | | | |
| LVDd (cm) | 0.40 ± 0.01 (10) | 0.40 ± 0.01 (10) | 0.37 ± 0.005 (10)[a] | 0.37 ± 0.01 (10)[a] |
| LVFS (%) | 27.05 ± 1.33 (10) | 26.03 ± 1.42 (10) | 32.72 ± 1.42 (10)[a] | 34.03 ± 1.26 (10)[a] |
| CO (ml/min) | 19.86 ± 1.40 (10) | 16.96 ± 0.86 (10) | 17.81 ± 0.83 (10) | 18.76 ± 1.59 (10) |

LVDd, LV diameter at end-diastole; LVFS, LV fractional shortening; CO, cardiac output. Values are the means ± SEM. *n* is indicated in parentheses.
[a]$P < 0.05$ versus room air determined using one way ANOVA with Bonferroni's multiple comparison test.
[b]$P < 0.05$ versus saline-treated group, determined using one way ANOVA with Bonferroni's multiple comparison test.

regulation of cytokine production (Kotlyarov et al., 1999). The duration and magnitude of activity of MAPKs like MK2 are determinants of its biological effect (Keyse, 2000). As an increase in p-p38 resulting from loss of BMPR2 caused heightened IL-6 production in PASMCs (Hagen et al., 2007), we investigated whether there was also enhanced mRNA translation of IL-6 in response to TNF. Indeed, a similar mechanism of prolonged p-p38 activation with reduced BMPR2 could explain heightened mRNA translation of both IL-6 and IL-8 in PAECs in response to TNF. We can only speculate as to why heightened translation of MCP-1 escapes modulation by prolonged p-p38 activation. Future studies could be aimed at identifying the subset of TNF-regulated transcripts that are differentially translated in response to loss of BMPR2, using microarray (Sampath et al., 2008) or RNA-Seq gene expression profiling in heavy versus light polysomes, correlated with proteomic analyses of cell lysates and conditioned media.

To connect prolonged activation of p-p38–MK2 with enhanced mRNA translation in association with TNF stimulation, we investigated whether assembly of stress granules was impaired under this condition. Stress granules are induced by inflammatory cytokines such as interferon-γ and TNF (Hu et al., 2010) to silence or dampen mRNA translation by mechanisms that include phosphorylation of eIF2α (Anderson and Kedersha, 2009). TNF treatment induced the phosphorylation of eIF2α, and this was inhibited by BMPR2 siRNA treatment in a p-p38–dependent manner. These data support impaired assembly of stress granules or stress granule disassembly as the mechanism involved in increasing GM-CSF mRNA translation. We speculated that p-p38 activated the GADD34–PP1 complex that promotes eIF2α dephosphorylation (Brush et al., 2003) and initiates mRNA translation. We did not find an increase in GADD34 and PP1 proteins, a mechanism previously related to heightened activity of the phosphatase complex (Oh-Hashi et al., 2001), nor did we find an increase in the formation of the complex between these proteins. We were able to show, however, that salubrinal, a selective inhibitor of GADD34–PP1 (Boyce et al., 2005), or lowering levels of PP1 by siRNA subverted the decrease in phosphorylated eIF2α, as well as the enhanced GM-CSF production attributed to reduced BMPR2. Thus, loss of BMPR2 likely activates GADD34–PP1 by a novel p-p38–dependent mechanism.

We confirmed, using immunofluorescence staining, that loss of BMPR2 could subvert stress granule formation induced by TNF or by other cellular stresses such as hypoxia. This observation implies that dysfunction of BMPR2 could interfere with stress granule formation in response to a wide variety of environmental stimuli implicated in the pathobiology of pulmonary hypertension (Speich et al., 1991; Cool et al., 2003; Stenmark et al., 2005; Marecki et al., 2006; Spiekerkoetter et al., 2008). It is possible, although unlikely, that despite the use of two different BMPR2 siRNAs and two different scrambled siRNAs, there were off-target effects independent of reducing BMPR2, which subverted stress granule assembly.

Once we confirmed heightened expression of GM-CSF in the PAs of patients with IPAH, we investigated whether this chemokine might be promoting the vascular pathology. GM-CSF was originally defined by its ability to generate granulocyte and macrophage colonies from bone marrow precursor cells after the proliferation and differentiation of these cells (Burgess and Metcalf, 1980). Later studies pursued the role of GM-CSF in regulating the function of more mature myeloid cells of granulocyte and macrophage lineages, during host defense and inflammatory reactions (Hamilton, 2008). For example, GM-CSF mediates macrophage polarization and induces production of the pro-inflammatory cytokines TNF, IL-6, and IL-12 (Fleetwood et al., 2007), as well as

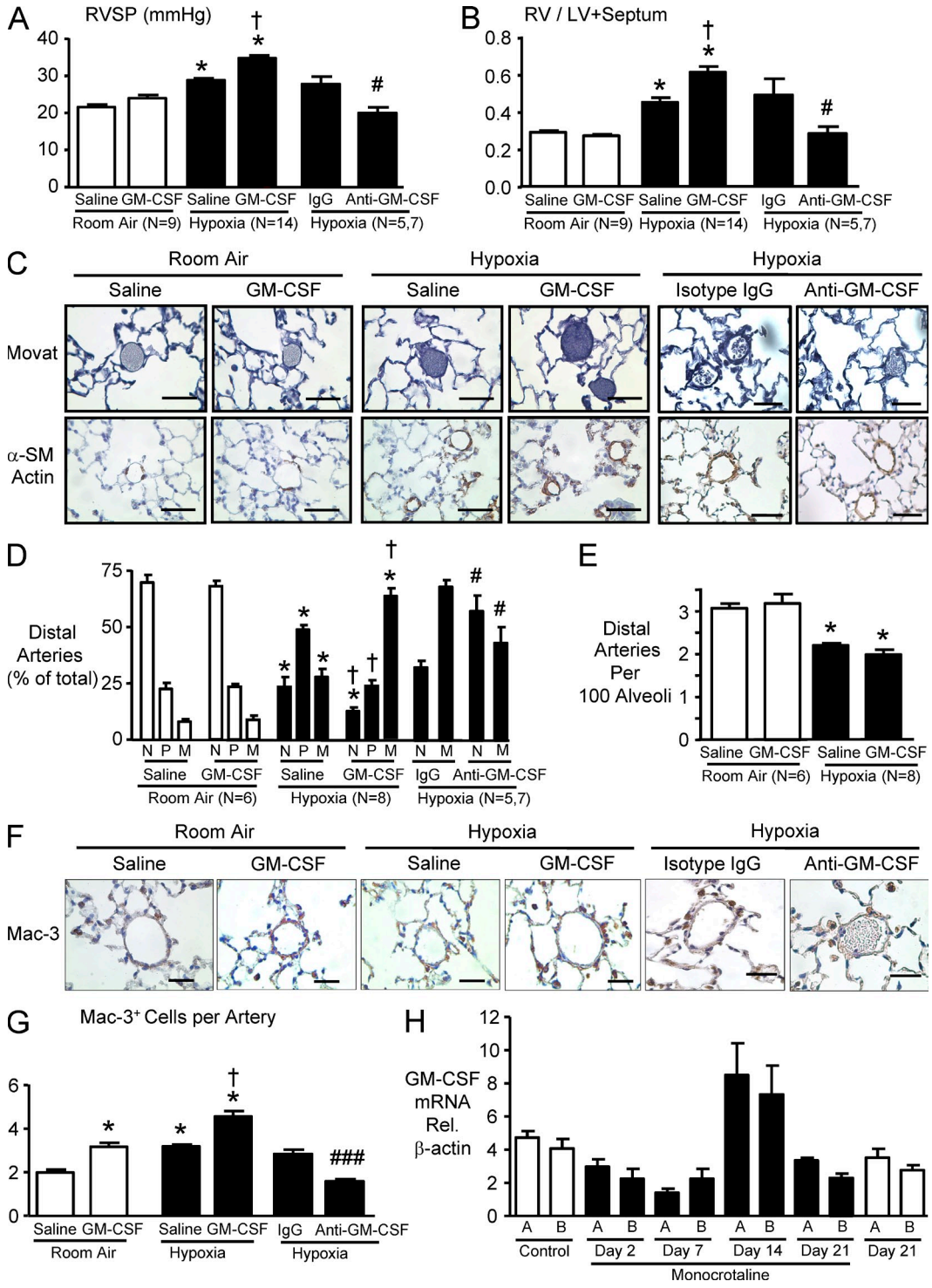


**Figure 8. GM-CSF exacerbates pulmonary hypertension induced by hypoxia in mice, and anti-GM-CSF reverses it.** C57BL/6 mice were exposed to hypoxia (10% oxygen) or kept in room air for 3 wk. Mice were injected with 0.4 µg/µl murine GM-CSF or saline, 5 d per week for 3 wk. In the second experiment, mice were exposed to hypoxia and treated with continuous s.c. anti-GM-CSF or 7 µg/ml isotype control as described in the Materials and methods. (A) RVSP. (B) Ratio of the RV to the LV plus septum. (C) Representative photomicrographs of barium-filled 15–50-µm alveolar wall and duct (distal) PAs. Muscularity of the distal PA was assessed by Movat pentachrome method (top) and immunostaining with α-SM–actin (bottom). Arteries are nonmuscular (N), partially muscular (P), or fully muscular (M), as described in Materials and methods. Room air distal arteries are mostly nonmuscular, whereas hypoxia vessels are mostly partially muscular and with GM-CSF treatment mostly fully muscular. (D) Percentage of N, P, and M arteries described in C was calculated for each group. In the anti–GM-CSF versus isotype control experiment M + P were pooled (M). (E) Distal PAs per 100 alveoli were counted in six randomly chosen lung fields per mouse, and the ratio was calculated comparing GM-CSF– and saline vehicle–injected control. (F) Representative

leukotriene B4 (Serezani et al., 2012), recently implicated in experimental and clinical PAH (Tian et al., 2013). GM-CSF responsiveness is not limited to hematopoietic lineages (Valdembri et al., 2009). ECs respond to GM-CSF and express both α and β subunits of the GM-CSF receptor (Soldi et al., 1997). GM-CSF–mediated EC activation induces both proliferation and expression of inflammatory cell adhesion molecules (Bussolino et al., 1989; Detmar et al., 1992). GM-CSF did not mediate proliferation of PAECs, and there was only a modest proliferation of PASMCs, in accordance with a previous report (Rolfe et al., 1995; unpublished data). Thus, other factors, i.e., GM-CSF–mediated recruitment of inflammatory or progenitor cells, may be relevant to the mechanism whereby GM-CSF promotes PAH or atherosclerosis (Haghighat et al., 2007) by inducing intimal cell proliferation in nascent lesions (Zhu et al., 2009).

We found heightened immunoreactivity for GM-CSF and GM-CSFRα in ECs and macrophages in IPAH PAs, and transcriptional analysis of single cells that express both CD31 and GM-CSFRα identified two subpopulations, one with endothelial and the other with monocyte/macrophage lineage markers. Collectively, it is conceivable that in the absence of normal BMPR2 signaling and in the presence of an inflammatory stimulus, an increase in GM-CSF induces GM-CSFRα–expressing PAECs and the recruitment of GM-CSFRα–positive inflammatory cells that induce adverse pulmonary vascular remodeling. It is also possible that an increase in GM-CSF converts a PASMC to a macrophage-like cell.

To address whether GM-CSF causes or exacerbates PAH, we investigated the effects of administering this chemokine to mice in room air or while exposed to chronic hypoxia. GM-CSF produced no evidence of PAH during treatment of the mice in room air but worsened hypoxia-induced PAH. Lung histology indicated that GM-CSF enhanced muscularization of distal arteries, which is consistent with its modest effect on proliferation of cultured SMCs that was observed by our group and others (Rolfe et al., 1995). It has also been shown that locally applied GM-CSF induces the accumulation of α-SM Actin–containing myofibroblasts (Rubbia-Brandt et al., 1991), and this, as well, could also explain the increased muscularization of distal vessels (Jones, 1992). More striking, however, was the observation that recruitment of perivascular macrophages or cells bearing a macrophage marker was amplified by GM-CSF. It has been suggested that macrophages can contribute to hypoxia-induced PAH (Stenmark et al., 2005; Vergadi et al., 2011) by enhancing cytokine production (Brissette et al., 1995; Li et al., 2011) and matrix metalloproteinase activity (Wu et al., 2001). That loss of BMPR2 per se does not aggravate hypoxia-induced PAH and associated vascular changes (Long et al., 2006), but does cause PAH in response to an inflammatory stimulus, suggests that greater loss of BMPR2 or a more severe hypoxia exposure may be necessary to bring out the subverted stress granule response that we see in cultured cells with both TNF as well as hypoxia. The reduction in stress granule formation is also more modest in response to hypoxia compared with TNF. Consistent with this, we showed that heightened production of GM-CSF is associated with progressive inflammatory forms of PAH, such as that induced by the toxin monocrotaline (Wilson et al., 1989). Heightened GM-CSF may also underlie the increased leukotriene B4 production by perivascular macrophages (Serezani et al., 2012), which is implicated in the inflammatory PAH produced in the athymic rat given VEGFR blockade (Tian et al., 2013), and in clinical PAH, which is also highly inflammatory (Humbert et al., 1995; Itoh et al., 2006; Soon et al., 2010).

## MATERIALS AND METHODS

**Materials and regents.** Recombinant human BMP-2, anti–α-tubulin antibody, anti–β-actin antibody, collagenase IA-S, protease inhibitor cocktail, and phosphatase inhibitor cocktails I and II were purchased from Sigma-Aldrich. Recombinant human TNF, GM-CSF, VEGF165, PDGF-BB, and mouse IgG were purchased from R&D Systems. BMPR2 and Mac-3 antibodies were purchased from BD, and S-6, L13a, p38, p-p38, MK2, p-MK2, I-κB, p–I-κB, eIF2α, and p-eIF2α antibodies were purchased from Cell Signaling Technology. GADD34, protein phosphatase-1, GM-CSFRα, HuR, and TIA-1 antibodies (4H1) and salubrinal were obtained from Santa Cruz Biotechnology, Inc., and G3BP antibody was obtained from BD. SB202190 was purchased from EMD Millipore. GM-CSF and TNF antibodies for immunohistochemistry were obtained from Abcam, and CD31, CD34, CD68, and α-SM actin antibodies and normal rabbit Ig were obtained from Dako. HRP-conjugated rabbit and mouse secondary antibodies and ECL and ECL Plus kits were ordered from GE Healthcare. Allophycocyanin (APC)-human CD31 and PE–GM-CSFRα antibodies were purchased from eBioscience. Recombinant murine GM-CSF was obtained from PeproTech.

**Cell culture.** Primary human PAECs from large vessels and human pulmonary microvascular ECs (PMVECs; ScienCell) were grown in commercial EC media (ScienCell), subcultured at a 1:6 ratio in gelatin-coated dishes and flasks (BD Falcon and Corning), and used at passages 4–6. Cells were starved in basal media (ScienCell) with 0.2% FBS and gentamycin/amphotericin overnight before adding the ligands or the vehicle. Primary human PASMCs from large vessels (Lonza) were grown in smooth muscle growth media-2 (Lonza), subcultured at a 1:3 ratio in uncoated flasks, and used at passages 4–6.

**ELISA for cytokines.** $2.5 \times 10^4$ cells were plated on 0.2% gelatin-coated 24-well plates and allowed to adhere for 24 h. Cells were washed in PBS and then starved in 0.2% FBS containing EC or SMC media for 24 h. After treatment with TNF, cell supernatants were collected and stored at −80°C.

immunostaining of lung tissue with the mouse macrophage marker Mac-3. Bars: (C) 50 µm; (F) 25 µm. (G) Mac-3$^+$ cells associated with the distal PAs were counted, and the means were calculated per mouse. For A, B, D, E, and G, bars represent mean ± SEM for *n* indicated in the panels (in the anti–GM-CSF experiment; $n = 5$ for isotype control and $n = 7$ for anti–GM-CSF). *, $P < 0.05$ versus room air control; †, $P < 0.05$ versus hypoxic mice injected with saline by one-way ANOVA with Bonferroni's multiple comparison test; and ###, $P < 0.001$ versus isotype IgG control by Student's *t* test. (H) Rats were injected with saline or 60 mg/kg of the toxin monocrotaline as described in Materials and methods, and GM-CSF mRNA relative to β-actin was assessed on days 0 and 21 in the saline controls and on days 2, 7, 14, and 21 in the monocrotaline group. A and B represent triplicate measurements in two different rats. Note values increase on day 14 by more than twofold relative to all other time points. Bars shown mean ± SEM.

The concentration of GM-CSF, IL-6, IL-8, and MCP-1 were determined using an ELISA kit (Quantikine; R&D Systems) according to the manufacturer's instructions.

**siRNA transfection.** siRNA specific for BMPR2 (Silencer Select; Ambion) or nontargeting siRNA as control (Silencer Select negative control; Ambion) were transfected into PAECs after withdrawal of antibiotics 24 h before and during treatment with Lipofectamine RNAi max (Invitrogen). Knockdown efficiency for BMPR2 was determined by Western immunoblot. We tested an additional control siRNA (Thermo Fisher Scientific) and two BMPR2 siRNAs (B2:s2045 and B3:s2046; Ambion) with similar results. Data shown were obtained with the siRNA (B1:s2044; Ambion). Knockdown efficiency, TNF-induced GM-CSF protein production, and TNF-induced phosphorylation of p38 and I-κB were analyzed and similar using either control or BMPR2 siRNA. We also performed experiments using siRNA specific for protein phosphatase 1c (s10930; Ambion).

**Western immunoblotting.** For protein expression analysis, PAECs or PMVECs were washed with ice-cold PBS, and lysates were prepared by adding boiling lysis buffer (10 mM Tris HCl, 1% SDS, and 0.2 mM PMSF) containing protease and phosphatase inhibitors. Lysates were scraped into a 1.5-ml microcentrifuge tube and boiled for 10 min before centrifugation. Supernatants were transferred to fresh microcentrifuge tubes and stored at −80°C. Protein concentration was determined by the Lowry assay (Bio-Rad Laboratories). Equal amounts of protein were loaded onto each lane of a 4–12% Bis-Tris gel and subjected to electrophoresis under reducing conditions. After blotting, polyvinylidene difluoride membranes were blocked for 1 h (5% milk powder in 0.1% PBS/Tween) and incubated with primary antibodies overnight at 4°C. The binding of secondary HRP-conjugated antibodies was visualized by ECL or ECL Plus. Normalizing for total protein was performed by reprobing the membrane with a mouse monoclonal antibody against α-tubulin or β-actin. The antibody dilutions used were 1:200 GM-CSF, 1:5,000 β-actin, 1:250 BMPR2, 1:1,000 p38, 1:1,000 p-p38, 1:1,000 MK2, 1:1,000 p-MK2, 1:1,000 I-κB, 1:1,000 p-I-κB, 1:1,000 eIF2α, 1:1,000 p-eIF2α, 1:200 GADD34 and PPI, and 1:5,000 α-tubulin. Secondary antibodies were used with dilutions of 1:2,000 to 1:10,000.

**qRT-PCR.** Total RNA was extracted and purified from cells using the RNeasy Mini kits (QIAGEN). The quantity and quality of RNA was determined by using a spectrophotometer, and 2 µg was used as the template for RT-PCR with random hexamers as primers. RT-PCR was performed on a 7900HT Sequence Detection System with TaqMan Gene Expression Assays on Demand probes (Applied Biosystems). Primers used are as follows: GM-CSF, Hs00171266_m1; β2 microglobulin, Hs99999907_m1; GAPDH, Hs02758991_m1; IL-6, Hs00985639_m1; IL-8, Hs00174103_m1; and MCP-1, Hs00234140_m1 (Applied Biosystems). In the monocrotaline experiments, RT-PCR for rat samples was performed by using 4 ng cDNA of whole lung lysate with 1 µl of 10 mM mixed primers, 5 µl SYBR green master mix (QIAGEN), and 4 µl sample. Primer sequences were designed using NCBI's Primer-BLAST function and are as follows: β-Actin (F, 5′-ACCCGCCACCAGTTCGCCAT-3′; R, 5′-CTTGCACATGCCGGAGCCGT-3′) and GM-CSF (F, 5′-GCTGCCCAACCCTGTCACC-3′; R, 5′-GGTTGCCCCGTAGACCCTGC-3′).

**mRNA stability.** After treating PAECs with 10 ng/ml TNF for 4 h, 20 µg/ml DRB was added to the media. GM-CSF mRNA levels were measured by qRT-PCR before and 20, 40, 60, 80, and 100 min after transcriptional inhibition by DRB.

**Polysome analysis.** Polysome analysis was performed as previously described (Ying et al., 2009; Wehner et al., 2010). PAECs transfected with siRNA for BMPR2 or control siRNA were stimulated with TNF for 3 h. Translation was inhibited with 0.1 mg/ml cycloheximide, and the cells were scraped and lysed in 500 µl lysis buffer (0.3 M NaCl, 15 mM $MgCl_2$, 15 mM Tris-HCl, pH 7.5, 1% Triton X-100, and 0.1 mg/ml cycloheximide) on ice for 10 min. Nuclei were pelleted at 10,000 *g* for 10 min, and 500 µl of the resulting supernatant was fractionated through a 10–60% linear sucrose gradient by centrifugation using a SW41 rotor for 2 h and 45 min at 35,000 rpm at 4°C. 15 fractions (750 µl each) were collected using a fraction collector (ISCO with Brandel pump). RNA in each fraction (650 µl) was extracted with phenol/chloroform/isoamyl alcohol (Invitrogen) and reverse-transcribed using Superscript III (Invitrogen). Real-time qPCR was performed on a 7900HT Sequence Detection System with TaqMan Gene Expression Assays on Demand probes. GAPDH was used as a housekeeping gene. Primers used are as follows: GM-CSF, Hs00171266_m1; and GAPDH, Hs99999907_m1 (Applied Biosystems). The amount of GM-CSF and GAPDH mRNA in each fraction was calculated. Protein was extracted from 100 µl of each polysome fraction by methanol for Western immunoblot analysis to detect the 40S ribosomal subunit protein S6 (1:1,000; 54D2; Cell Signaling Technology) and the 60S ribosomal subunit protein L13a (1:1,000; Cell Signaling Technology).

**Immunofluorescent staining for stress granule formation.** Stress granule formation was assessed as previously described (Kedersha and Anderson, 2007). $5 \times 10^4$ PAECs were plated on a 4-well chamber slide. After serum starvation for 12 h, cells were treated with vehicle or 10 ng/ml TNF for 3 h. To assess stress granule formation after hypoxia, cells were incubated in a hypoxic chamber (1% $O_2$) and studied under the same conditions. In all experiments, the cells were fixed with 4% paraformaldehyde for 15 min and then treated with methanol for 10 min. After blocking with 5% horse serum, slides were incubated with an antibody against G3BP, the protein which is known to assemble stress granules (Tourrière et al., 2003), followed by Alexa Fluor 594–conjugated secondary antibody. Sections were stained with DAPI (Invitrogen) to visualize nuclei and mounted with Prolong Gold Antifade Reagent. Stress granule formation was assessed using fluorescence and confocal microscopy (FluoView 1000; Olympus). Stress granule–positive cells were counted relative to total cells in three randomly chosen high-power fields in four different experiments.

**Lung tissues from IPAH patients and unused donor lungs.** Lung tissues from IPAH patients who underwent lung transplantation and from unused donor lungs as controls were obtained through the Pulmonary Hypertension Breakthrough Initiative (PHBI) Network, which is funded by the Cardiovascular Medical Research and Education Fund (CMREF). The tissues were procured at the Transplant Procurement Centers at Allegheny General Hospital, Baylor University, Cleveland Clinic, Duke University, Stanford University, the University of California, San Diego, University of Alabama at Birmingham, and Vanderbilt University, and de-identified patient data were obtained via the Data Coordinating Center at the University of Michigan. Lung tissues were kept in RPMI 1640 media supplemented with antibiotics for up to 24 h during transportation from the transplant procurement centers. Small pieces of the lung tissue were snap-frozen in liquid nitrogen and stored at −80°C for biochemical experiments or fixed in 10% formaldehyde overnight for immunohistochemistry. Procurement of the tissues from human subjects is approved by the Administrative Panel on Human Subjects in Medical Research at Stanford University (IRB #350, Panel 6).

**Immunohistochemistry.** Human and mouse sections from formaldehyde-fixed and paraffin-embedded lung tissues were deparaffinized and rehydrated. Epitope retrieval was performed by boiling the sections in citrate buffer, pH 6.0. Sections were reacted with hydrogen peroxide to block endogenous peroxidase, washed, and blocked with 5% goat serum. The sections were then incubated with the primary antibodies against GM-CSF (1:400; Abcam), TNF (1:400; Abcam), α-SM actin (1:1; Dako), CD31 (1:50; Dako), CD34 (1:1; Dako), CD68 (1:100; Dako), GM-CSFRα (1:50; Santa Cruz Biotechnology, Inc.), and Mac3 (1:200; BD) overnight at 4°C. After streptavidin-biotin amplification (LSAB2 kit [Dako] or Vectastain Elite ABC kit [Vector Laboratories]), the slides were incubated with 3, 3′-diaminobenzidine and counterstained with hematoxylin. A negative control was performed using mouse IgG or rabbit Ig instead of the primary antibody. The localization and

intensity (0, 1+, 2+, 3+) of immunoreactivity were assessed by two independent examiners, blinded to the diagnosis of PAH or to the mouse treatment group. In the murine experiments described below, the number of Mac-3–positive cells per PA was counted for all vessels in the section and a mean value calculated per mouse.

**PAEC and PASMC proliferation assays.** Proliferation was assessed by cell counts. Human PAECs or PMVECs were seeded at $2.5 \times 10^4$ cells per well in a gelatin-coated 24-well plate in a 500-µl volume of growth medium and allowed to adhere for 24 h. Cells were washed three times and starved in 0.2% FBS containing EC media for 12 h and then incubated for 24 h in the presence or absence of the different ligands. Cells were counted in a hemocytometer (Bright-Line; Hausser Scientific). PASMCs were seeded as described above but starved in 0.1% FBS for 48 h before stimulation.

**Cell isolation from lung tissue.** Left lung sections (3 × 3 × 2 cm) were transported in RPMI 1640 medium, then chopped into small pieces (1 × 1 × 2 mm) using scissors, and placed in a 50-ml conical tube. The minced tissue was digested in 20 ml HBSS (Gibco) containing 0.8 mg/ml collagenase IA-S (Sigma-Aldrich) on the rotator platform for 45 min at 37°C. The cell suspension was filtered using a cell strainer (100 µm, Falcon; BD) and centrifuged at 250 *g* for 5 min. The pellet was resuspended in 2∼4 ml of PBS containing 0.1% BSA. Magnetic beads (30 µl, Dynabeads; Invitrogen) conjugated with anti-CD31 antibody were added and incubated with the cell suspension for 20 min at 4°C. The cells bound to the beads were recovered with a magnet rack (Dynal) and washed five times with PBS containing 0.1% BSA. The cells were counted with a hemocytometer, and up to $2 \times 10^6$ cells were used for FACS.

**FACS analysis and sorting.** After blocking nonspecific binding with media containing 5% FBS for 15 min on ice, cell suspensions were centrifuged at 250 *g* for 5 min, resuspended in 100 µl FACS buffer (0.2% fetal bovine serum, 2 mM EDTA, and PBS, pH 7.2) containing APC-conjugated CD31 and PE-conjugated GM-CSFRα antibodies, and incubated on ice for 20 min. Then cells were washed with 0.1% BSA/PBS, resuspended in FACS buffer, and analyzed and sorted using a multiparameter cell sorter (FACS Aria, BD). Single cells from subpopulations of $CD31^+GM\text{-}CSFR\alpha^-$ or $CD31^+GM\text{-}CSFR\alpha^+$ cells were sorted into a 96-well plate that had been preloaded with RT-PCR reagents (reverse transcription enzyme and primers) for each gene target.

**Microfluidic-based single cell transcriptional analysis.** As previously described (Thorsen et al., 2002; Diehn et al., 2009), single cells were sorted into each well of a 96-well plate that had been preloaded with 10 µl of a master mix containing Tris-EDTA buffer, pH 7.0, Superscript III Platinum reverse transcription/Taq DNA polymerase enzyme mix (Invitrogen), Cells Direct reaction mix (Invitrogen), target gene–specific TaqMan assay (primer/probe) sets (Applied Biosystems), and SUPERase-In RNase inhibitor (Applied Biosystems). Exon-spanning primers were used where possible to avoid amplification of genomic background. Reverse transcription was performed (20 min at 50°C, 2 min at 95°C), followed immediately by a 22-cycle preamplification in the same reaction tube (denature at 95°C for 15 min, anneal at 60°C for 4 min, each cycle). Resultant single cell cDNA was mixed with sample loading agent (Fluidigm) and Universal PCR Master Mix (Applied Biosystems) and loaded into 48.48 Dynamic Array chips (Fluidigm) along with TaqMan gene expression assays and assay loading agent (Fluidigm). Products were analyzed on the BioMark reader system (Fluidigm) using a hot start protocol to minimize primer-dimer formation. 30 RT-PCR cycles were performed. Gene expression data from all individual cells were normalized relative to the median expression for each gene in the pooled sample and converted to base 2 logarithms. Absolute bounds of ±5 cycle thresholds (corresponding to 32-fold increases/decreases in expression) were set, and zero-expressers were assigned to this floor. After normalization of datasets from multiple chip runs, a pooled analysis was used to examine the characteristics of the entire population of cells. To detect overlapping patterns within the single cell transcriptional data, we used an adaptive fuzzy c-means clustering algorithm for partitioning of the cells based on similar transcriptional profiles (Glotzbach et al., 2011).

**Animal experiments.** The Animal Care Committee of Stanford University approved all protocols, in keeping with the regulations of the American Physiological Society.

**GM-CSF administration to mice exposed to hypoxia.** 8-wk-old C57BL/6 mice were exposed to 10% oxygen or kept in ambient air, and both groups were either treated with a daily i.p. injection of GM-CSF (0.4 µg/dose; PeproTech) or saline vehicle for five consecutive days per week, for 3 wk using a protocol previously described (Haghighat et al., 2007). Subgroups in normoxia and hypoxia were treated for 2 wk with continuous s.c. administration of 7 µg/d rat anti–mouse GM-CSF–IgG (eBioscience) or unspecific isotype control rat IgG2a (eBioscience) via s.c. mini-osmotic pump (model 1002; Alzet).

**Monocrotaline administration to rats.** 12 male Sprague Dawley rats (220–280 g) were randomly selected for a single injection with 60 mg/kg monocrotaline (8 animals) or 0.9% saline (4 animals). Lungs of the control animals were harvested at days 0 and 21, and lungs of monocrotaline-treated animals were harvested at days 2, 7, 14, and 21 for whole lung lysate mRNA extraction.

**Echocardiography.** After 20 d of GM-CSF treatment, cardiac function and output were measured by echocardiography under isoflurane anesthesia (1%, 1 liter/min oxygen) using a Vivid 7 ultrasound machine (GE Healthcare) and a 13-MHz linear array transducer as in our previous study (Hansmann et al., 2008).

**RVSP measurements.** RVSP was measured under isoflurane anesthesia (1.5%, 1 liter/min oxygen) by inserting a 1.4F catheter (Millar Instruments) via the right jugular vein as previously described (Hansmann et al., 2008). Pressure measurements were repeated three times and the mean value used. Data were collected by Power Lab Data Acquisition system (AD Instruments) and analyzed using LabChart software (AD Instruments) by an investigator blinded to the treatment group.

**Hematological experiments.** A blood sample was taken by heart puncture after the completion of the RVSP measurement, and a complete blood cell count that included a differential count of white blood cells was performed in the diagnostic laboratory of the Stanford Animal Care Facility.

**RV hypertrophy.** RV hypertrophy was assessed by the weight of the RV relative to LV plus septum.

**Tissue preparation for the histological experiments.** After the hemodynamic measurements were completed, the isolated lungs were perfused with saline, fixed in 10% formalin overnight, and then embedded in paraffin for immunohistochemistry. Mac-3–positive cells adherent to the distal alveolar duct and wall PAs were counted in a full-length section of each lung, and a mean was calculated for each mouse. A subset of left lungs was prepared for morphometric analysis of the vasculature, using the barium injection method that has been reported in detail (Guignabert et al., 2009).

**Morphometric analysis.** Sections parallel to the hilum in the mid-portion of the barium-injected left lung were taken and embedded in the same manner and stained by the Movat pentachrome method. All barium-filled arteries 15–50 µm in external diameter at alveolar duct and alveolar wall level were assessed for the presence of muscularity. These distal PAs and alveoli were counted in six randomly chosen lung fields per mouse, and the ratio of the number of distal PAs to 100 alveoli was calculated. All measurements were performed by two investigators blinded to the experimental group being studied.

**Statistical analysis.** Values from multiple experiments are shown as mean ± SEM. Statistical significance was determined using one-way ANOVA followed by Bonferroni's multiple comparison test. When only two groups were compared, statistical differences were assessed with unpaired two-tailed Student's *t* test. A p-value of $<0.05$ was considered significant. The number of samples or animals in each group is indicated in the figures or figure legends.

We greatly appreciate the editorial and technical assistance of Dr. Michal Bental Roof in preparing both the manuscript and figures and the administrative help of Ms. Michelle Fox. Lung tissues from IPAH and control patients were provided by the PHBI, which is funded by the CMREF. The tissues were procured at the Transplant Procurement Centers at Baylor University, Stanford University, University of California, San Diego, and Vanderbilt University, and de-identified patient data were obtained via the Data Coordinating Center at the University of Michigan.

This work was supported by grants from the National Institutes of Health National Heart, Lung, and Blood Institute (R01 HL087118 and N01-HV-00242 HHSN268201000034C to M. Rabinovitch). H. Sawada was supported by a grant from Mie University Graduate School of Medicine and from the Oak Foundation, J.P. Glotzbach by the Oak Foundation, R. Chan by a studentship and Y.-M. Kim by a fellowship from the American Heart Association, N.P. Nickel by a fellowship from the German Research Foundation (DFG), T.-P. Alastalo by the Sigrid Juselius Foundation, Instrumentarium Foundation, Finnish Foundation for Cardiovascular Research, Finnish Cultural Foundation, Finnish Foundation for Pediatric Research, and the Academy of Finland, and V. de Jesus Perez by a grant from the Amos Foundation. M. Rabinovitch was supported by the Dunlevie Chair of Pediatric Cardiology at Stanford University.

The authors have no conflicting financial interests.

**Submitted: 18 August 2011**
**Accepted: 13 December 2013**

## REFERENCES

Alastalo, T.P., M. Li, V.J. Perez, D. Pham, H. Sawada, J.K. Wang, M. Koskenvuo, L. Wang, B.A. Freeman, H.Y. Chang, and M. Rabinovitch. 2011. Disruption of PPARγ/β-catenin-mediated regulation of apelin impairs BMP-induced mouse and human pulmonary arterial EC survival. *J. Clin. Invest.* 121:3735–3746. http://dx.doi.org/10.1172/JCI43382

Anderson, P., and N. Kedersha. 2008. Stress granules: the Tao of RNA triage. *Trends Biochem. Sci.* 33:141–150. http://dx.doi.org/10.1016/j.tibs.2007.12.003

Anderson, P., and N. Kedersha. 2009. RNA granules: post-transcriptional and epigenetic modulators of gene expression. *Nat. Rev. Mol. Cell Biol.* 10:430–436. http://dx.doi.org/10.1038/nrm2694

Asosingh, K., M.A. Aldred, A. Vasanji, J. Drazba, J. Sharp, C. Farver, S.A. Comhair, W. Xu, L. Licina, L. Huang, et al. 2008. Circulating angiogenic precursors in idiopathic pulmonary arterial hypertension. *Am. J. Pathol.* 172:615–627. http://dx.doi.org/10.2353/ajpath.2008.070705

Atkinson, C., S. Stewart, P.D. Upton, R. Machado, J.R. Thomson, R.C. Trembath, and N.W. Morrell. 2002. Primary pulmonary hypertension is associated with reduced pulmonary vascular expression of type II bone morphogenetic protein receptor. *Circulation.* 105:1672–1678. http://dx.doi.org/10.1161/01.CIR.0000012754.72951.3D

Boyce, M., K.F. Bryant, C. Jousse, K. Long, H.P. Harding, D. Scheuner, R.J. Kaufman, D. Ma, D.M. Coen, D. Ron, and J. Yuan. 2005. A selective inhibitor of eIF2alpha dephosphorylation protects cells from ER stress. *Science.* 307:935–939. http://dx.doi.org/10.1126/science.1101902

Brissette, W.H., D.A. Baker, E.J. Stam, J.P. Umland, and R.J. Griffiths. 1995. GM-CSF rapidly primes mice for enhanced cytokine production in response to LPS and TNF. *Cytokine.* 7:291–295. http://dx.doi.org/10.1006/cyto.1995.0035

Brown, J.A., T.L. Roberts, R. Richards, R. Woods, G. Birrell, Y.C. Lim, S. Ohno, A. Yamashita, R.T. Abraham, N. Gueven, and M.F. Lavin. 2011. A novel role for hSMG-1 in stress granule formation. *Mol. Cell. Biol.* 31:4417–4429. http://dx.doi.org/10.1128/MCB.05987-11

Brush, M.H., D.C. Weiser, and S. Shenolikar. 2003. Growth arrest and DNA damage-inducible protein GADD34 targets protein phosphatase 1 alpha to the endoplasmic reticulum and promotes dephosphorylation of the alpha subunit of eukaryotic translation initiation factor 2. *Mol. Cell. Biol.* 23:1292–1303. http://dx.doi.org/10.1128/MCB.23.4.1292-1303.2003

Burgess, A.W., and D. Metcalf. 1980. The nature and action of granulocyte-macrophage colony stimulating factors. *Blood.* 56:947–958.

Bussolino, F., J.M. Wang, P. Defilippi, F. Turrini, F. Sanavio, C.J. Edgell, M. Aglietta, P. Arese, and A. Mantovani. 1989. Granulocyte- and granulocyte-macrophage-colony stimulating factors induce human endothelial cells to migrate and proliferate. *Nature.* 337:471–473. http://dx.doi.org/10.1038/337471a0

Cool, C.D., P.R. Rai, M.E. Yeager, D. Hernandez-Saavedra, A.E. Serls, T.M. Bull, M.W. Geraci, K.K. Brown, J.M. Routes, R.M. Tuder, and N.F. Voelkel. 2003. Expression of human herpesvirus 8 in primary pulmonary hypertension. *N. Engl. J. Med.* 349:1113–1122. http://dx.doi.org/10.1056/NEJMoa035115

Crane, I.J., M.C. Kuppner, S. McKillop-Smith, C.A. Wallace, and J.V. Forrester. 1999. Cytokine regulation of granulocyte-macrophage colony-stimulating factor (GM-CSF) production by human retinal pigment epithelial cells. *Clin. Exp. Immunol.* 115:288–293.

Davie, N.J., J.T. Crossno Jr., M.G. Frid, S.E. Hofmeister, J.T. Reeves, D.M. Hyde, T.C. Carpenter, J.A. Brunetti, I.K. McNiece, and K.R. Stenmark. 2004. Hypoxia-induced pulmonary artery adventitial remodeling and neovascularization: contribution of progenitor cells. *Am. J. Physiol. Lung Cell. Mol. Physiol.* 286:L668–L678. http://dx.doi.org/10.1152/ajplung.00108.2003

Detmar, M., S. Tenorio, U. Hettmannsperger, Z. Ruszczak, and C.E. Orfanos. 1992. Cytokine regulation of proliferation and ICAM-1 expression of human dermal microvascular endothelial cells in vitro. *J. Invest. Dermatol.* 98:147–153. http://dx.doi.org/10.1111/1523-1747.ep12555746

Diehn, M., R.W. Cho, N.A. Lobo, T. Kalisky, M.J. Dorie, A.N. Kulp, D. Qian, J.S. Lam, L.E. Ailles, M. Wong, et al. 2009. Association of reactive oxygen species levels and radioresistance in cancer stem cells. *Nature.* 458:780–783. http://dx.doi.org/10.1038/nature07733

Fleetwood, A.J., T. Lawrence, J.A. Hamilton, and A.D. Cook. 2007. Granulocyte-macrophage colony-stimulating factor (CSF) and macrophage CSF-dependent macrophage phenotypes display differences in cytokine profiles and transcription factor activities: implications for CSF blockade in inflammation. *J. Immunol.* 178:5245–5252.

Frid, M.G., J.A. Brunetti, D.L. Burke, T.C. Carpenter, N.J. Davie, J.T. Reeves, M.T. Roedersheimer, N. van Rooijen, and K.R. Stenmark. 2006. Hypoxia-induced pulmonary vascular remodeling requires recruitment of circulating mesenchymal precursors of a monocyte/macrophage lineage. *Am. J. Pathol.* 168:659–669. http://dx.doi.org/10.2353/ajpath.2006.050599

Fujita, M., R.J. Mason, C. Cool, J.M. Shannon, N. Hara, and K.A. Fagan. 2002. Pulmonary hypertension in TNF-alpha-overexpressing mice is associated with decreased VEGF gene expression. *J. Appl. Physiol.* 93:2162–2170.

Glotzbach, J.P., M. Januszyk, I.N. Vial, V.W. Wong, A. Gelbard, T. Kalisky, H. Thangarajah, M.T. Longaker, S.R. Quake, G. Chu, and G.C. Gurtner. 2011. An information theoretic, microfluidic-based single cell analysis permits identification of subpopulations among putatively homogeneous stem cells. *PLoS ONE.* 6:e21211. http://dx.doi.org/10.1371/journal.pone.0021211

Guignabert, C., C.M. Alvira, T.P. Alastalo, H. Sawada, G. Hansmann, M. Zhao, L. Wang, N. El-Bizri, and M. Rabinovitch. 2009. Tie2-mediated loss of peroxisome proliferator-activated receptor-gamma in mice causes PDGF receptor-beta-dependent pulmonary arterial muscularization. *Am. J. Physiol. Lung Cell. Mol. Physiol.* 297:L1082–L1090. http://dx.doi.org/10.1152/ajplung.00199.2009

Hagen, M., K. Fagan, W. Steudel, M. Carr, K. Lane, D.M. Rodman, and J. West. 2007. Interaction of interleukin-6 and the BMP pathway in pulmonary smooth muscle. *Am. J. Physiol. Lung Cell. Mol. Physiol.* 292:L1473–L1479. http://dx.doi.org/10.1152/ajplung.00197.2006

Haghighat, A., D. Weiss, M.K. Whalin, D.P. Cowan, and W.R. Taylor. 2007. Granulocyte colony-stimulating factor and granulocyte macrophage colony-stimulating factor exacerbate atherosclerosis in apolipoprotein E-deficient mice. *Circulation.* 115:2049–2054. http://dx.doi.org/10.1161/CIRCULATIONAHA.106.665570

Hamilton, J.A. 2008. Colony-stimulating factors in inflammation and autoimmunity. *Nat. Rev. Immunol.* 8:533–544. http://dx.doi.org/10.1038/nri2356

Hansmann, G., V.A. de Jesus Perez, T.P. Alastalo, C.M. Alvira, C. Guignabert, J.M. Bekker, S. Schellong, T. Urashima, L. Wang, N.W. Morrell, and M. Rabinovitch. 2008. An antiproliferative BMP-2/PPARgamma/apoE axis in human and murine SMCs and its role in pulmonary hypertension. *J. Clin. Invest.* 118:1846–1857. http://dx.doi.org/10.1172/JCI32503

Hitti, E., T. Iakovleva, M. Brook, S. Deppenmeier, A.D. Gruber, D. Radzioch, A.R. Clark, P.J. Blackshear, A. Kotlyarov, and M. Gaestel. 2006. Mitogen-activated protein kinase-activated protein kinase 2 regulates tumor necrosis factor mRNA stability and translation mainly by altering tristetraprolin expression, stability, and binding to adenine/uridine-rich element. *Mol. Cell. Biol.* 26:2399–2407. http://dx.doi.org/10.1128/MCB.26.6.2399-2407.2006

Hong, K.H., Y.J. Lee, E. Lee, S.O. Park, C. Han, H. Beppu, E. Li, M.K. Raizada, K.D. Bloch, and S.P. Oh. 2008. Genetic ablation of the BMPR2 gene in pulmonary endothelium is sufficient to predispose to pulmonary arterial hypertension. *Circulation.* 118:722–730. http://dx.doi.org/10.1161/CIRCULATIONAHA.107.736801

Hu, S., E.C. Claud, M.W. Musch, and E.B. Chang. 2010. Stress granule formation mediates the inhibition of colonic Hsp70 translation by interferon-gamma and tumor necrosis factor-alpha. *Am. J. Physiol. Gastrointest. Liver Physiol.* 298:G481–G492. http://dx.doi.org/10.1152/ajpgi.00234.2009

Humbert, M., G. Monti, F. Brenot, O. Sitbon, A. Portier, L. Grangeot-Keros, P. Duroux, P. Galanaud, G. Simonneau, and D. Emilie. 1995. Increased interleukin-1 and interleukin-6 serum concentrations in severe primary pulmonary hypertension. *Am. J. Respir. Crit. Care Med.* 151:1628–1631. http://dx.doi.org/10.1164/ajrccm.151.5.7735624

Itoh, T., N. Nagaya, H. Ishibashi-Ueda, S. Kyotani, H. Oya, F. Sakamaki, H. Kimura, and N. Nakanishi. 2006. Increased plasma monocyte chemoattractant protein-1 level in idiopathic pulmonary arterial hypertension. *Respirology.* 11:158–163. http://dx.doi.org/10.1111/j.1440-1843.2006.00821.x

Jones, R. 1992. Ultrastructural analysis of contractile cell development in lung microvessels in hyperoxic pulmonary hypertension. Fibroblasts and intermediate cells selectively reorganize nonmuscular segments. *Am. J. Pathol.* 141:1491–1505.

Kedersha, N., and P. Anderson. 2007. Mammalian stress granules and processing bodies. *Methods Enzymol.* 431:61–81.

Keyse, S.M. 2000. Protein phosphatases and the regulation of mitogen-activated protein kinase signalling. *Curr. Opin. Cell Biol.* 12:186–192. http://dx.doi.org/10.1016/S0955-0674(99)00075-7

Kotlyarov, A., A. Neininger, C. Schubert, R. Eckert, C. Birchmeier, H.D. Volk, and M. Gaestel. 1999. MAPKAP kinase 2 is essential for LPS-induced TNF-alpha biosynthesis. *Nat. Cell Biol.* 1:94–97. http://dx.doi.org/10.1038/10061

Lane, K.B., R.D. Machado, M.W. Pauciulo, J.R. Thomson, J.A. Phillips III, J.E. Loyd, W.C. Nichols, and R.C. Trembath; International PPH Consortium. 2000. Heterozygous germline mutations in BMPR2, encoding a TGF-beta receptor, cause familial primary pulmonary hypertension. *Nat. Genet.* 26:81–84. http://dx.doi.org/10.1038/79226

Li, M., S.R. Riddle, M.G. Frid, K.C. El Kasmi, T.A. McKinsey, R.J. Sokol, D. Strassheim, B. Meyrick, M.E. Yeager, A.R. Flockton, et al. 2011. Emergence of fibroblasts with a proinflammatory epigenetically altered phenotype in severe hypoxic pulmonary hypertension. *J. Immunol.* 187:2711–2722. http://dx.doi.org/10.4049/jimmunol.1100479

Long, L., M.R. MacLean, T.K. Jeffery, I. Morecroft, X. Yang, N. Rudarakanchana, M. Southwood, V. James, R.C. Trembath, and N.W. Morrell. 2006. Serotonin increases susceptibility to pulmonary hypertension in BMPR2-deficient mice. *Circ. Res.* 98:818–827. http://dx.doi.org/10.1161/01.RES.0000215809.47923.fd

Marecki, J.C., C.D. Cool, J.E. Parr, V.E. Beckey, P.A. Luciw, A.F. Tarantal, A. Carville, R.P. Shannon, A. Cota-Gomez, R.M. Tuder, et al. 2006. HIV-1 Nef is associated with complex pulmonary vascular lesions in SHIV-nef-infected macaques. *Am. J. Respir. Crit. Care Med.* 174:437–445. http://dx.doi.org/10.1164/rccm.200601-005OC

Newman, J.H., R.C. Trembath, J.A. Morse, E. Grunig, J.E. Loyd, S. Adnot, F. Coccolo, C. Ventura, J.A. Phillips III, J.A. Knowles, et al. 2004. Genetic basis of pulmonary arterial hypertension: current understanding and future directions. *J. Am. Coll. Cardiol.* 43:S33–S39. http://dx.doi.org/10.1016/j.jacc.2004.02.028

Oh-Hashi, K., W. Maruyama, and K. Isobe. 2001. Peroxynitrite induces GADD34, 45, and 153 VIA p38 MAPK in human neuroblastoma SH-SY5Y cells. *Free Radic. Biol. Med.* 30:213–221. http://dx.doi.org/10.1016/S0891-5849(00)00461-5

Perros, F., P. Dorfmüller, D. Montani, H. Hammad, W. Waelput, B. Girerd, N. Raymond, O. Mercier, S. Mussot, S. Cohen-Kaminsky, et al. 2012. Pulmonary lymphoid neogenesis in idiopathic pulmonary arterial hypertension. *Am. J. Respir. Crit. Care Med.* 185:311–321. http://dx.doi.org/10.1164/rccm.201105-0927OC

Pietra, G.G., W.D. Edwards, J.M. Kay, S. Rich, J. Kernis, B. Schloo, S.M. Ayres, E.H. Bergofsky, B.H. Brundage, K.M. Detre, et al. 1989. Histopathology of primary pulmonary hypertension. A qualitative and quantitative study of pulmonary blood vessels from 58 patients in the National Heart, Lung, and Blood Institute, Primary Pulmonary Hypertension Registry. *Circulation.* 80:1198–1206. http://dx.doi.org/10.1161/01.CIR.80.5.1198

Rolfe, B.E., J.H. Campbell, N.J. Smith, M.W. Cheong, and G.R. Campbell. 1995. T lymphocytes affect smooth muscle cell phenotype and proliferation. *Arterioscler. Thromb. Vasc. Biol.* 15:1204–1210. http://dx.doi.org/10.1161/01.ATV.15.8.1204

Rosborough, B.R., A. Castellaneta, S. Natarajan, A.W. Thomson, and H.R. Turnquist. 2012. Histone deacetylase inhibition facilitates GM-CSF-mediated expansion of myeloid-derived suppressor cells in vitro and in vivo. *J. Leukoc. Biol.* 91:701–709.

Rosenberg, H.C., and M. Rabinovitch. 1988. Endothelial injury and vascular reactivity in monocrotaline pulmonary hypertension. *Am. J. Physiol.* 255:H1484–H1491.

Rubbia-Brandt, L., A.P. Sappino, and G. Gabbiani. 1991. Locally applied GM-CSF induces the accumulation of alpha-smooth muscle actin containing myofibroblasts. *Virchows Arch. B Cell Pathol. Incl. Mol. Pathol.* 60:73–82. http://dx.doi.org/10.1007/BF02899530

Sampath, P., D.K. Pritchard, L. Pabon, H. Reinecke, S.M. Schwartz, D.R. Morris, and C.E. Murry. 2008. A hierarchical network controls protein translation during murine embryonic stem cell self-renewal and differentiation. *Cell Stem Cell.* 2:448–460. http://dx.doi.org/10.1016/j.stem.2008.03.013

Serezani, C.H., S. Kane, L. Collins, M. Morato-Marques, J.J. Osterholzer, and M. Peters-Golden. 2012. Macrophage dectin-1 expression is controlled by leukotriene B4 via a GM-CSF/PU.1 axis. *J. Immunol.* 189:906–915. http://dx.doi.org/10.4049/jimmunol.1200257

Soldi, R., L. Primo, M.F. Brizzi, F. Sanavio, M. Aglietta, N. Polentarutti, L. Pegoraro, A. Mantovani, and F. Bussolino. 1997. Activation of JAK2 in human vascular endothelial cells by granulocyte-macrophage colony-stimulating factor. *Blood.* 89:863–872.

Song, Y., J.E. Jones, H. Beppu, J.F. Keaney Jr., J. Loscalzo, and Y.Y. Zhang. 2005. Increased susceptibility to pulmonary hypertension in heterozygous BMPR2-mutant mice. *Circulation.* 112:553–562. http://dx.doi.org/10.1161/CIRCULATIONAHA.104.492488

Soon, E., A.M. Holmes, C.M. Treacy, N.J. Doughty, L. Southgate, R.D. Machado, R.C. Trembath, S. Jennings, L. Barker, P. Nicklin, et al. 2010. Elevated levels of inflammatory cytokines predict survival in idiopathic and familial pulmonary arterial hypertension. *Circulation.* 122:920–927. http://dx.doi.org/10.1161/CIRCULATIONAHA.109.933762

Speich, R., R. Jenni, M. Opravil, M. Pfab, and E.W. Russi. 1991. Primary pulmonary hypertension in HIV infection. *Chest.* 100:1268–1271. http://dx.doi.org/10.1378/chest.100.5.1268

Spiekerkoetter, E., C.M. Alvira, Y.M. Kim, A. Bruneau, K.L. Pricola, L. Wang, N. Ambartsumian, and M. Rabinovitch. 2008. Reactivation of gammaHV68 induces neointimal lesions in pulmonary arteries of S100A4/Mts1-overexpressing mice in association with degradation of elastin. *Am. J. Physiol. Lung Cell. Mol. Physiol.* 294:L276–L289. http://dx.doi.org/10.1152/ajplung.00414.2007

Steiner, M.K., O.L. Syrkina, N. Kolliputi, E.J. Mark, C.A. Hales, and A.B. Waxman. 2009. Interleukin-6 overexpression induces pulmonary hypertension.

*Circ. Res.* 104:236–244. http://dx.doi.org/10.1161/CIRCRESAHA.108.182014

Stenmark, K.R., N.J. Davie, J.T. Reeves, and M.G. Frid. 2005. Hypoxia, leukocytes, and the pulmonary circulation. *J. Appl. Physiol.* 98:715–721. http://dx.doi.org/10.1152/japplphysiol.00840.2004

Stevens, T., P.L. Janssen, and A.D. Tucker. 1992. Acute and long-term TNF-alpha administration increases pulmonary vascular reactivity in isolated rat lungs. *J. Appl. Physiol.* 73:708–712.

Takahashi, T., C. Kalka, H. Masuda, D. Chen, M. Silver, M. Kearney, M. Magner, J.M. Isner, and T. Asahara. 1999. Ischemia- and cytokine-induced mobilization of bone marrow-derived endothelial progenitor cells for neovascularization. *Nat. Med.* 5:434–438. http://dx.doi.org/10.1038/7434

Tamosiuniene, R., W. Tian, G. Dhillon, L. Wang, Y.K. Sung, L. Gera, A.J. Patterson, R. Agrawal, M. Rabinovitch, K. Ambler, et al. 2011. Regulatory T cells limit vascular endothelial injury and prevent pulmonary hypertension. *Circ. Res.* 109:867–879. http://dx.doi.org/10.1161/CIRCRESAHA.110.236927

Thenappan, T., A. Goel, G. Marsboom, Y.H. Fang, P.T. Toth, H.J. Zhang, H. Kajimoto, Z. Hong, J. Paul, C. Wietholt, et al. 2011. A central role for CD68(+) macrophages in hepatopulmonary syndrome. Reversal by macrophage depletion. *Am. J. Respir. Crit. Care Med.* 183:1080–1091. http://dx.doi.org/10.1164/rccm.201008-1303OC

Thorsen, T., S.J. Maerkl, and S.R. Quake. 2002. Microfluidic large-scale integration. *Science.* 298:580–584. http://dx.doi.org/10.1126/science.1076996

Tian, W., X. Jiang, R. Tamosiuniene, Y.K. Sung, J. Qian, G. Dhillon, L. Gera, L. Farkas, M. Rabinovitch, R.T. Zamanian, et al. 2013. Blocking macrophage leukotriene b4 prevents endothelial injury and reverses pulmonary hypertension. *Sci. Transl. Med.* 5:200ra117. http://dx.doi.org/10.1126/scitranslmed.3006674

Toren, A., and A. Nagler. 1998. The implications of granulocyte-monocyte colony-stimulating factor (GM-CSF) in cytotoxicity of bone marrow transplantation. *Cytokines Cell. Mol. Ther.* 4:199–206.

Tourrière, H., K. Chebli, L. Zekri, B. Courselaud, J.M. Blanchard, E. Bertrand, and J. Tazi. 2003. The RasGAP-associated endoribonuclease G3BP assembles stress granules. *J. Cell Biol.* 160:823–831. http://dx.doi.org/10.1083/jcb.200212128

Tuder, R.M., B. Groves, D.B. Badesch, and N.F. Voelkel. 1994. Exuberant endothelial cell growth and elements of inflammation are present in plexiform lesions of pulmonary hypertension. *Am. J. Pathol.* 144:275–285.

Valdembri, D., P.T. Caswell, K.I. Anderson, J.P. Schwarz, I. König, E. Astanina, F. Caccavari, J.C. Norman, M.J. Humphries, F. Bussolino, and G. Serini. 2009. Neuropilin-1/GIPC1 signaling regulates alpha-5beta1 integrin traffic and function in endothelial cells. *PLoS Biol.* 7:e25. http://dx.doi.org/10.1371/journal.pbio.1000025

Vergadi, E., M.S. Chang, C. Lee, O.D. Liang, X. Liu, A. Fernandez-Gonzalez, S.A. Mitsialis, and S. Kourembanas. 2011. Early macrophage recruitment and alternative activation are critical for the later development of hypoxia-induced pulmonary hypertension. *Circulation.* 123:1986–1995. http://dx.doi.org/10.1161/CIRCULATIONAHA.110.978627

Wehner, K.A., S. Schütz, and P. Sarnow. 2010. OGFOD1, a novel modulator of eukaryotic translation initiation factor 2alpha phosphorylation and the cellular response to stress. *Mol. Cell. Biol.* 30:2006–2016. http://dx.doi.org/10.1128/MCB.01350-09

Wilson, D.W., H.J. Segall, L.C. Pan, and S.K. Dunston. 1989. Progressive inflammatory and structural changes in the pulmonary vasculature of monocrotaline-treated rats. *Microvasc. Res.* 38:57–80. http://dx.doi.org/10.1016/0026-2862(89)90017-4

Wu, L., A. Tanimoto, Y. Murata, J. Fan, Y. Sasaguri, and T. Watanabe. 2001. Induction of human matrix metalloproteinase-12 gene transcriptional activity by GM-CSF requires the AP-1 binding site in human U937 monocytic cells. *Biochem. Biophys. Res. Commun.* 285:300–307. http://dx.doi.org/10.1006/bbrc.2001.5161

Yeager, M.E., C.M. Nguyen, D.D. Belchenko, K.L. Colvin, S. Takatsuki, D.D. Ivy, and K.R. Stenmark. 2012. Circulating myeloid-derived suppressor cells are increased and activated in pulmonary hypertension. *Chest.* 141:944–952.

Ying, L., A. Lau, C.M. Alvira, R. West, G.M. Cann, B. Zhou, C. Kinnear, E. Jan, P. Sarnow, M. Van de Rijn, and M. Rabinovitch. 2009. LC3-mediated fibronectin mRNA translation induces fibrosarcoma growth by increasing connective tissue growth factor. *J. Cell Sci.* 122:1441–1451. http://dx.doi.org/10.1242/jcs.025957

Zhu, S.N., M. Chen, J. Jongstra-Bilen, and M.I. Cybulsky. 2009. GM-CSF regulates intimal cell proliferation in nascent atherosclerotic lesions. *J. Exp. Med.* 206:2141–2149. http://dx.doi.org/10.1084/jem.20090866